

ORIGINAL RESEARCH PAPER

Thermo-mechanical Buckling Analysis of Non-homogeneous Open Circular Cylindrical Shells Reinforced with Single-walled Carbon Nanotubes

H.R. Balali Dehkordi, Y. Tadi Beni*, R. Balali Dehkordi, P. Mohammadi Dashtaki

Department of Mechanical Engineering, Shahrekord University, Shahrekord, Iran.

Article info

Article history:

Received 05 November 2021

Received in revised form

31 December 2021

Accepted 03 January 2022

Keywords:

Mechanical buckling

Thermal buckling

Open cylindrical shell

Carbon nanotubes

Third-order theory of shear deformation

Abstract

In this paper, the thermo-mechanical buckling analysis of a non-homogeneous open cylindrical shell reinforced with single-walled carbon nanotubes with a uniform/non-uniform distribution on an elastic foundation under thermal and mechanical loads has been addressed. Using the minimum energy principle, the governing differential equations of this system are derived and in order to determine the properties of the reinforced composite shell, the modified mixtures law has been used. It is assumed that the properties of single-walled carbon nanotubes are acquired from molecular dynamics simulation. It is also assumed that the material properties of the reinforced carbon nanotube composites are linear in the thickness and are defined based on mixture law via a micro-mechanical model in which the nanotube performance parameter is considered. After solving these equations, the effects of geometric characteristics of the shell and material properties on the critical load and critical temperature of shell buckling are investigated.

Nomenclature

w_{CNT}	Mass fraction of carbon nanotubes	μ'	Variation coefficient
ρ_{CNT}	Density of carbon nanotubes	ν^m	Poisson's ratio of matrix media
ρ_m	Density of matrix media	ν_{12}^{CNT}	Poisson's ratio of carbon nanotubes
V_{CNT}	Volume fraction of carbon nanotubes	u, v, w	Displacements of cylindrical shell
V_m	Volume fraction of matrix media	$\varepsilon_\theta, \varepsilon_x$	Normal strains
a	Radius of the middle plane	$\gamma_{x\theta}, \gamma_{xz}, \gamma_{\theta z}$	Shear strains
E_{11}^{CNT}	Young's modulus of carbon nanotubes	$\tau_{\theta z}, \tau_{xz}, \tau_{x\theta}$	Shear stresses
E_{22}^{CNT}	Young's modulus of carbon nanotubes	h	Thickness of cylindrical shell
α_{11}^{CNT}	Coefficient of thermal expansion of carbon nanotubes	α_{22}^{CNT}	Coefficient of thermal expansion of carbon nanotubes
L	Length of cylindrical shell	θ	Opening angle of cylindrical shell
G_{12}^{CNT}	Shear modulus of carbon nanotubes	σ_x, σ_θ	Normal stresses
E^m	Young's modulus of matrix	E_0	Elasticity modulus of homogeneous shell
G^m	Shear modulus of matrix	Q_{ij}	Stiffness matrix components
α^m	Matrix coefficient of thermal expansion	N_i, M_i, P_i	Normal stress resultants
η_j	Coefficient of productivity	Q_i, R_i	Shear stress resultants

*Corresponding author: Y. Tadi Beni (Professor)

E-mail address: Tadi@sku.ac.ir

<http://dx.doi.org/10.22084/JRSTAN.2021.24830.1192>

ISSN: 2588-2597

K_w	Winkler coefficient	U	Strain energy
K_g	Pasternak coefficient	V	Total potential energy
U_T	Energy caused by thermal strain	Ω	Work of external forces
U_f	Energy caused by the elastic foundation		

1. Introduction

A group of materials called carbon nanotubes has recently attracted particular attention. Via conduction of specific experiments and simulations; it is understood that these nanotubes have better mechanical properties than carbon fibers [1]. Since the mechanical attributes of composites depend on the behavior of fibers inside them, the former carbon fibers can be replaced with carbon nanotubes. This process can improve the properties of composites, such as tensile strength and elastic modulus.

Most research on carbon nanotube-reinforced composites has focused on material properties. Various studies have shown that adding a small percentage of nanotubes to a matrix significantly increases the electrical, mechanical, and thermal properties of composites [2–6]. Kordani et al. [7] showed that the stiffness of carbon nanotube-reinforced composite beams could be improved by uniform diffusion of a small percentage of nanotubes. Vodenitcharova and Zhang [8] studied the bending of reinforced carbon nanotube composite beams. Formica et al. [9] studied the behavior of vibration in the reinforced carbon nanotube composite plates by expending an equivalent continuous model according to the Mori Tanaka method.

Experiments and studies on carbon nanotube-reinforced composite have shown that the uniform distribution of nanotubes as reinforcements in the matrix causes a moderate improvement in mechanical properties [10, 11]. Another type of nanotube distribution in carbon nanotube-reinforced composites is the non-homogeneous distribution of carbon nanotubes with a specific slope to improve the composite's buckling behavior. Shen [12] found that the non-linear bending behavior can be improved by the functional gradient (FG) distribution of carbon nanotubes in the matrix. Shen and Zhu [13] also investigated the effect of carbon nanotubes on the post-buckling and heat post-buckling behavior of functionally graded nanotube-reinforced composite plates. Ke et al. [14] studied the vibrations of reinforced Timoshenko FG-beams with carbon nanotubes. It was established that for the linear/non-linear frequencies of the FG repartition, carbon nanotubes were higher than the uniform distribution (UD) or asymmetric distribution state of the nanotubes. Raufi et al. [15] studied the vibrations of an FG two-dimensional perforated sector plate with the elastic foundation. It was established that the power law's constants and the elastic basis have important effects on the frequencies of the system. Moreover, in structures made of 2D functionally gradient materials, us-

ing more parameters, the vibrational of the system can be controlled compared to one-dimensional functionally gradient materials. Mohammadimehr et al. [16] studied the effect of heat on deflection, buckling load of Euler-Bernoulli beam vibrations on the Pasternak foundation using the Ritz method. It was established that with increasing Winkler-type spring constant and Pasternak shear constant, the amount of deflection in the beam decreases, and the natural frequency and critical load increase. With increasing temperature, the deflection rate increases, and the critical buckling load and natural frequency decrease.

Pourasghar et al. conducted the three-dimensional analysis of cylindrical shells with temperature-dependent properties reinforced with carbon nanotubes which were subjected to ambient temperature. Using the generalized differential quadrature method solution method, they obtained an accurate solution for thermoelastic analysis of cylindrical shells reinforced with carbon nanotubes [17]. Ghorbanpour Arani et al. investigated the buckling of the piezoelectric cylindrical shell reinforced with DWBNNT nanotubes under electro-thermomechanical load. This study has shown that the use of reverse voltage or decreasing the temperature increases the critical load. furthermore, piezoelectricity generally increases the buckling resistance of the composite cylindrical shell [18]. Using the HDQM method, Mosalaei Barzoki et al. investigated the non-linear buckling response of the piezoelectric cylindrical shell reinforced with BNNT materials electro-thermomechanical load. The results show that in comparison with other non-intelligent materials such as CNTs, the presence of piezoelectricity increases the critical load in composites [19].

Mohammadi et al. conducted a thermoelastic analysis of FG pressure vessels reinforced with carbon nanotubes based on different Pasternak foundation patterns. The governing relations have been achieved by utilizing the principle of virtual work under fixed boundary conditions. Therefore, the various parameters effect similar to the volume fraction of nanotubes and Pasternak coefficients and the type of arrangement pattern of nanotubes have been explored [21]. Additionally, Arefi et al. did a two-dimensional thermoelastic analysis of FG pressure vessel reinforced with carbon nanotubes using first-order shear deformation theory [22]. Arefi et al. analyzed the passive vibrations of FG sandwich reinforced beams with carbon nanotubes in the magnetic and thermal environment using non-local strain gradient theory and various theories of shear deformation [23]. They conducted a non-local bending analysis of a curved nano-beam re-

inforced with graphene nanoplatelets according to the first-order shear deformation theory (FSDT). The results displayed that the number of graphene layers has a special effect on displacements and stresses [24]. Furthermore, Arefi et al. studied the size-dependent free vibrations of a graphene-reinforced polymer composite beam located on a Pasternak foundation. In this paper, FSDT is utilized, and the law of mixtures and Halpin-Tsai model are applied to analyze the mechanical attributes of the composite. This study shows that increasing the stiffness ratio with graphene nanoplatelets to its length increases the natural frequency [25]. Arefi et al. studied the free vibrations of a graphene-reinforced polymer nanoplate based on two-variable shear deformation theory and a non-linear elastic theory, which was also considered transversely as the sum of the variables of bending and shear deformation. Obtained numerical results displayed that according to the higher flexural strength of composite materials, the FG-X pattern for such graphenes had the maximum natural frequency [26].

Tadi Beni et al. [27] analyzed the free vibrations of simply supported functionally graded cylindrical nanoshells, using the modified couple stress theory in conjunction with the first order shear deformation shell model. General equations of motion were solved by the Navier procedure for the special case of simply supported functionally graded cylindrical nanoshells [27]. Mehralian and Tadi Beni [28] investigated the size dependent torsional buckling behavior of cylindrical shell made of through-the-thickness functionally graded materials, and the modified couple stress shell theory with the von Karman geometrical nonlinearity was utilized to derive the governing equations and boundary conditions based on the minimum potential energy principle. As a special case, the torsional buckling of simply supported and clamped FG cylindrical shells was examined using the GDQ method.

Mehralian et al. [29] developed the size-dependent formulation of shear deformable Functionally Graded Piezoelectric (FGP) cylindrical nanoshells based on a new modified couple stress theory to study the buckling of simply supported FGP cylindrical nanoshells under uniform lateral external pressure. Zeighampour and Tadi Beni [30] studied the wave propagation in functionally graded carbon nanotube reinforced composite (FG CNTRC) cylindrical microshell by taking into consideration nonlocal constant and material length scale parameter. Shear deformable shell theory as well as nonlocal strain gradient theory and Hamilton's principle were used to drive classical governing equations of the FG CNTRC cylindrical microshell and UD and FG-X Carbon nanotubes distributions were investigated.

Mohammad Dashtaki and Tadi Beni [31] investigated the thermal and size effects on the buckling behavior of a nanobeam symmetrically located between two electrodes, subjected to the influence of the nonlin-

ear external forces including electrostatic and Casimir attractions.

Song et al. [32] investigated the wave dispersion characteristics of graphene reinforced nanocomposite curved viscoelastic panels. The second-order shear deformation theory in curvilinear coordinate was used to develop the doubly-curved shell as a continuous structure and the general nonlocal strain gradient theory was adopted to calculate nonlocality and strain gradient size-dependency. Khorasani et al. [33] studied the vibration analysis of graphene nanoplatelets reinforced composite plates integrated by piezo-electromagnetic patches on the piezo-electromagnetic media by sinusoidal shear deformation plate theory.

Karimi Zeverdejani et al. [34] presented the buckling and post-buckling of graphene-reinforced laminated composite plates subjected to uniaxial and biaxial loadings. Governing Equations of motion of the plate were modeled using the first shear deformation theory and for large deformation, von Karman nonlinearity was considered. Mechanical properties of each layer were evaluated using the molecular dynamics simulation [34]. Karimi Zeverdejani and Tadi Beni [35] investigated the effect of laminate configuration on the free vibration/buckling of FG Graphene/PMMA composites. Buckling and free vibration of rectangular polymeric laminate reinforced by graphene sheets were investigated by considering various patterns for augmentation of each laminate.

Bagherizadeh et al. [36] studied the mechanical buckling of functionally graded material cylindrical shell that was embedded in an outer elastic medium and subjected to combined axial and radial compressive loads based on Higher-order Shear Deformation Shell Theory (HSDT) considering the transverse shear strains. Babaei and Eslami [37] investigated the nonlinear static bending behavior of infinite length cylindrical panels made of Functionally Graded Porous (FGP) materials with clamped edges and subjected to uniform temperature rise and transverse pressure loading. Nosier and Ruhi [38] presented a semi-analytical solution for three dimensional elastic analysis of finitely long, simply supported, orthotropic, laminated cylindrical panels with piezoelectric layers subjected to outer pressure and electrostatic excitation.

Because of the wide need for shell structures with high thermal and mechanical reinforcement in aerospace industries, this study focuses on the thermo-mechanical buckling of composite carbon nanotubes reinforced cylindrical shells under axial pressure and temperature. The main problem here is calculating the load and buckling temperature for reinforced composite cylindrical shells with carbon nanotubes under different volume fractions of the nanotubes. It is supposed that the properties of single-walled carbon nanotubes (SWCNs) depend on temperature and size effect from MD simulations. It is also supposed that

the properties of the reinforced composites with carbon nanotubes are graded in the thickness direction and are defined by the law of mixtures. Stability equations are also obtained from the neighborhood method of adjacent points by making a rise in displacement components. The obtained equations are explained using the wave method, and the various parameters affecting the thermo-mechanical buckling are investigated. The novelty of the present research is to investigate the non-homogeneity effect of mechanical properties by using the third order shear deformation theory and also the effect of elastic substrate and different nano tubes distributions on the thermo-mechanical buckling parameters of a cylindrical panel.

2. Mechanical Properties of Reinforced Composite with Carbon Nanotubes

Based on the previous research on the properties of nanocomposites among various mechanical models, the Mori Tanaka model has been very accurate. On the other hand, the modified rule of mixtures due to simplicity and convenience and excellent compliance with the Mori Tanaka model has been the most used in recent research in nanocomposites. Therefore, as mentioned earlier, in the present research, the modified rule of mixtures has been used to determine the properties of reinforced nanocomposites. By showing the properties of the matrix with index m and the properties of reinforcing particles with index f , the related equations to the volume fraction are as follows [20]:

$$\begin{aligned} V_{CNT} &= w(z) V_{CNT}^* \\ V_{CNT}^* &= \frac{w_{CNT}}{w_{CNT} + \frac{\rho_{CNT}}{\rho_m} - \frac{\rho_{CNT}}{\rho_m} (w_{CNT})} \\ V_{CNT} + V_m &= 1 \end{aligned} \quad (1)$$

where w_{CNT} , ρ_{CNT} , ρ_m , V_{CNT} , and V_m are mass fraction of carbon nanotubes, density of carbon nanotubes, density of matrix media, volume fraction of carbon nanotubes, and volume fraction of matrix media, respectively. According to the conducted research, there are different distributions of carbon nanotubes in the matrix body, volume fraction of the various distributions are given in the following equations [26].

$$V_{CNT}(z) = V_{CNT}^* (UD - CNTRC) \quad (2)$$

$$V_{CNT}(z) = \left(1 + \frac{2Z}{h}\right) V_{CNT}^* (FG - V CNTRC) \quad (3)$$

$$V_{CNT}(z) = 2 \left(1 - \frac{2|Z|}{h}\right) V_{CNT}^* (FG - O CNTRC) \quad (4)$$

$$V_{CNT}(z) = 2 \left(\frac{2|Z|}{h}\right) V_{CNT}^* (FG - X CNTRC) \quad (5)$$

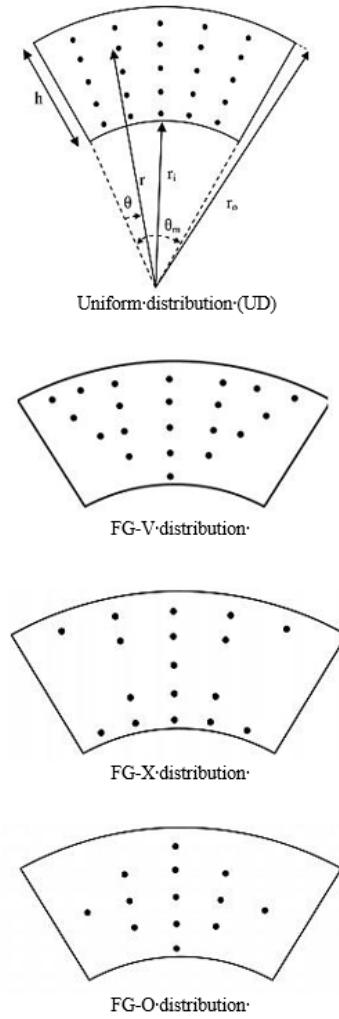


Fig. 1. Schematic of the carbon nanotubes distribution.

According to the rule of mixtures, the following equations are proposed for the modulus of longitudinal and shear elasticity [20, 39]:

$$\begin{aligned} E^m &= E_0 \left(1 + \mu' \frac{z}{h}\right) \\ E_{11} &= \eta_1 V_{CNT} E_{11}^{CNT} + V_m E^m \\ \frac{\eta_3}{E_{22}} &= \frac{V_{CNT}}{E_{22}^{CNT}} + \frac{V_m}{E^m} \\ \frac{\eta_3}{G_{12}} &= \frac{V_{CNT}}{G_{12}^{CNT}} + \frac{V_m}{G^m} \\ G^m &= \frac{E^m}{2(1 + \nu^m)} \\ \alpha_{11} &= V_{CNT} \alpha_{11}^{CNT} + V_m \alpha^m \\ \alpha_{22} &= (1 + \nu_{12}^{CNT}) V_{CNT} \alpha_{22}^{CNT} + (1 + \nu^m) V_m \alpha^m \\ &\quad - \nu_{12} \alpha^{11} \end{aligned} \quad (6)$$

where E_0 is the modulus of the elasticity of the homogeneous shell, E_{11}^{CNT} and E_{22}^{CNT} is Young's modulus and α_{11}^{CNT} and α_{22}^{CNT} is the coefficient of thermal

expansion and G_{12}^{CNT} is the shear modulus of carbon nanotubes. E^m and G^m and α^m are also properties related to the matrix. η_j is called the coefficient of productivity or efficiency of the nanotube calculated by merging the elastic modulus of the composite reinforced with the carbon nanotube from the molecular dynamics method with the numerical results obtained from the rule of mixtures. μ' is the variation coefficient that varies from zero to one. Poisson's ratio, ν_{12} , is slightly dependent on temperature and position as follows:

$$\nu_{12} = V_{CNT}^* \nu_{12}^{CNT} + V_m \nu^m \quad (7)$$

3. Modeling the Problem and Its Governing Equations

Based on Fig. 2, the shell of open cylinders is considered with the radius of the middle plate a , the thickness h , and the length L ; the coordinate system (x, θ, z) where x is considered in the direction of the axis of the shell, θ in the tangential direction, and z in the vertical direction on the middle surface.

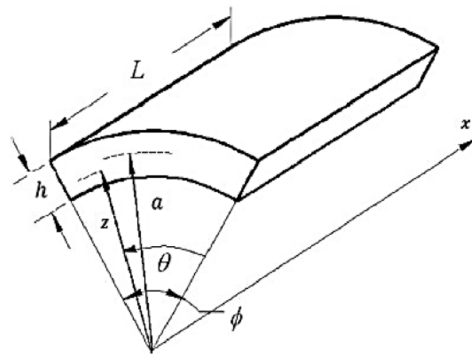


Fig. 2. The geometry of the cylindrical panel and the coordinate system intended for it.

Strain-displacement relations based on Donnell non-linear theory are [40]:

$$\begin{aligned} \varepsilon_x &= u_{0,x} + \frac{1}{2} w_{,x}^2, \\ \varepsilon_\theta &= \frac{v_{0,\theta} + w}{a} + \frac{1}{2} \left(\frac{+w_{,\theta}}{a} \right)^2, \\ \gamma_{x\theta} &= \frac{u_{0,\theta}}{a} + v_{0,x} + \frac{w_{,x} w_{,\theta}}{a}, \\ \gamma_{xz} &= u_1 + w_{,x}, \quad \gamma_{\theta z} = v_1 + \frac{w_{,\theta}}{a} - \frac{v_0}{a} \end{aligned} \quad (8)$$

ε_θ , ε_x are vertical strains and $\gamma_{x\theta}$, γ_{xz} and $\gamma_{\theta z}$ are shear strains, and comma strains represent partial derivatives. Furthermore, u , v , and w are the displacement of the cylindrical shell in the directions x , θ , and z , respectively.

There are various theories to study the kinematics of beam deformation. One of the most widely used

is the Euler-Bernoulli classical beam theory. In this theory, the straight line perpendicular to the neutral axis of the beam remains straight and perpendicular to the neutral axis after the deformation of the beam. In other words, this theory ignores the effects of transverse shear strains, which are valid for beams with a high length-to-width ratio. Overcoming this limitation of Euler-Bernoulli's theory, Timoshenko's theory is applied. In this theory, the effects of transverse shear strain are considered. In fact, in Timoshenko's theory of beams, a correction factor is required that depends on the geometrical and material parameters of the structure. Disadvantages of this theory include non-zero strain conditions at free surfaces. Correcting Timoshenko's beam theory, high-order shear theories were developed that consider the shear strain distribution in the beam thickness direction, so that boundary conditions are established on free surfaces. In other words, the zero-strain condition is established at free surfaces without the need to consider the correction factor. One of the disadvantages of the mentioned theories is that the normal strain in the thickness direction is not considered. In these theories, the normal strain in the direction of the thickness of the structure is considered zero. In other words, the length of the element remains constant in the direction of the thickness of the structure before deformation and after deformation, which is, of course, correct for structures with low thickness. Zenkour has proposed a modified theory in which he considers the effects of both shear strain and normal stress in the direction of thickness. In a study by Zenkour and Arefi, using non-local beam theory that considers the effects of normal deformation and transverse shear, they conducted a thermo-mechanical analysis of a nano-beam with a core and with functional gradient properties and two piezomagnetic layers. In another study, Zenkour and Arefi studied the free vibrations of a three-layer microbeam consisting of an elastic microcore and two piezomagnetic layers located on the Pasternak foundation. In their research, a three-parameter kinematic theory was used, which considers the effects of normal deformation and transverse shear [41–43]:

Considering the Third-Order Shear Deformation Theory, the assumption that the rotational inertia and lateral shear strains γ_{xz} and $\gamma_{\theta z}$ are negligible is not valid, and only the normal strain component ε_z is considered zero. The displacement field of the cylindrical shell according to the Third-Order Shear Deformation Theory is as follows [44–46]:

$$\begin{aligned} u(x, \theta, z) &= u_0(x, \theta) + z u_1(x, \theta) + z^2 u_2(x, \theta) \\ &\quad + z^3 u_3(x, \theta) \\ v(x, \theta, z) &= v_0(x, \theta) + z v_1(x, \theta) + z^2 v_2(x, \theta) \\ &\quad + z^3 v_3(x, \theta) \\ w(x, \theta, z) &= w(x, \theta) \end{aligned} \quad (9)$$

u_0 , v_0 , and w_0 define displacements of midplane surface of the panel at ($z = 0$) in the x , θ , and z directions, and u_1 and v_1 are respectively the rotations of the mid-plane surface around the x and θ axes. Satisfying the zero shear strain condition at the boundary surfaces of the panel $\gamma_{\theta z}(x, \theta, \pm \frac{h}{2}) = 0$ and $\gamma_{xz}(x, \theta, \pm \frac{h}{2}) = 0$ and using the approximation $(1 + \frac{h}{a}) \cong 1$, Eq. (9) is rewritten as follows:

$$\begin{aligned} u(x, \theta, z) &= u_0 + zu_1 - c_0 z^3 (u_1 + w_{,x}) \\ v(x, \theta, z) &= v_0 + zv_1 - c_0 z^3 \left(v_1 + \frac{w_{,\theta}}{a} \right) \\ w(x, \theta, z) &= w(x, \theta) \end{aligned} \quad (10)$$

where coefficient C_0 in Eq. (10) is defined as $C_0 = \frac{4}{3h^2}$. By substituting Eq. (10) in the displacement strain relations (8), the kinematic relations are as follows:

$$\begin{aligned} \varepsilon_{xx} &= \varepsilon_x + zk_x + z^3 k_1 \\ \varepsilon_{\theta\theta} &= \varepsilon_\theta + zk_\theta + z^3 k_2 \\ \gamma_{x\theta} &= \gamma_{x\theta} + 2zk_{x\theta} + 2z^3 k_3 \\ \gamma_{xz} &= \gamma_{xz} + 2z^2 k_{xz} \\ \gamma_{\theta z} &= \gamma_{\theta z} + 2z^2 k_{\theta z} \\ \varepsilon_{zz} &= 0 \end{aligned} \quad (11)$$

where:

$$\begin{aligned} \begin{Bmatrix} \varepsilon_{xm} \\ \varepsilon_{\theta m} \\ \gamma_{x\theta m} \\ \gamma_{xz m} \\ \gamma_{\theta z m} \end{Bmatrix} &= \begin{Bmatrix} u_{0,x} + \frac{1}{2}w_{,x}^2 \\ \frac{v_{0,\theta} + w}{a} + \frac{1}{2}\left(\frac{-w_{,\theta}}{a}\right)^2 \\ \frac{u_{0,\theta}}{a} + v_{0,x} + \left(\frac{+w_{,x}w_{,\theta}}{a}\right) \\ u_1 + w_{,x} \\ v_1 + \frac{w_{,\theta}}{a} \end{Bmatrix}, \\ \begin{Bmatrix} k_x \\ k_\theta \\ k_{x\theta} \\ k_{xz} \\ k_{\theta z} \end{Bmatrix} &= \begin{Bmatrix} \frac{u_{1,x}}{a} \\ \frac{v_{1,\theta}}{a} \\ \frac{1}{2}\left(\frac{u_{1,\theta}}{a} + v_{1,x}\right) \\ -\frac{3c_0}{2}(u_1 + w_{,x}) \\ -\frac{3c_0}{2}\left(v_1 + \frac{w_{,\theta}}{a}\right) \end{Bmatrix}, \\ \begin{Bmatrix} k_1 \\ k_2 \\ k_3 \end{Bmatrix} &= \begin{Bmatrix} -c_0(u_{1,x} + w_{,xx}) \\ -\frac{c_0}{a}\left(v_{1,\theta} + \frac{w_{,\theta\theta}}{a}\right) \\ -\frac{c_0}{2}\left(\frac{u_{1,\theta}}{a} + v_{1,x} + \frac{2w_{,x\theta}}{a}\right) \end{Bmatrix} \end{aligned} \quad (12)$$

Therefore, the non-linear strain- displacement relation is as follows:

$$\begin{aligned} \varepsilon_{xx} &= u_{0,x} + \frac{1}{2}w_{,x}^2 + zu_{1,x} - c_0 z^3 (u_{1,x} + w_{,xx}) \\ \varepsilon_{\theta\theta} &= \frac{v_{0,\theta} + w}{a} = \frac{1}{2}\left(\frac{-w_{,\theta}}{a}\right)^2 + \frac{zv_{1,\theta}}{a} \\ &\quad - \frac{c_0}{a} z^3 \left(v_{1,\theta} + \frac{w_{,\theta\theta}}{a} \right) \\ \gamma_{x\theta} &= \frac{u_{0,\theta}}{a} + v_{0,x} + \left(\frac{+w_{,x}w_{,\theta}}{a}\right) + z\left(\frac{u_{1,\theta}}{a} + v_{1,x}\right) \end{aligned} \quad (13)$$

$$\begin{aligned} &- c_0 z^3 \left(\frac{u_{1,\theta}}{a} + v_{1,x} + \frac{2w_{,x\theta}}{a} \right) \\ \gamma_{xz} &= w_{,x} + u_1 - 3c_0 z^2 (u_1 + w_{,x}) \\ \gamma_{\theta z} &= \frac{1}{a} w_{,\theta} + v_1 - 3c_0 z^2 \left(v_1 + \frac{w_{,\theta}}{a} \right) \end{aligned}$$

Moreover, the stress-strain relations for orthotropic plates are as follows [47]:

$$\begin{Bmatrix} \sigma_x \\ \sigma_\theta \\ \tau_{\theta z} \\ \tau_{xz} \\ \tau_{x\theta} \end{Bmatrix} = \begin{bmatrix} Q_{11} & Q_{12} & 0 & 0 & 0 \\ Q_{21} & Q_{22} & 0 & 0 & 0 \\ 0 & 0 & Q_{44} & 0 & 0 \\ 0 & 0 & 0 & Q_{55} & 0 \\ 0 & 0 & 0 & 0 & Q_{66} \end{bmatrix} \begin{Bmatrix} \varepsilon_{xx} - \alpha_{11}\Delta T \\ \varepsilon_{\theta\theta} - \alpha_{22}\Delta T \\ \gamma_{\theta z} \\ \gamma_{xz} \\ \gamma_{x\theta} \end{Bmatrix} \quad (14)$$

where Q is the stiffness matrix, and its values are defined as follows [47, 48]:

$$\begin{aligned} Q_{11} &= \frac{E_{11}}{1 - \nu_{12}\nu_{21}}, \\ Q_{12} &= \frac{\nu_{21}E_{11}}{1 - \nu_{12}\nu_{21}}, \\ Q_{22} &= \frac{E_{22}}{1 - \nu_{12}\nu_{21}}, \\ Q_{66} &= G_{12}, \\ Q_{55} &= G_{13} \\ Q_{44} &= G_{23}, \end{aligned} \quad (15)$$

In Eq. (10), the coefficients G_{12} , ν_{12} , ν_{21} , E_{22} , E_{11} , and G_{23} are calculated from the modified rule of mixtures. The resulting forces and moments are defined as follows [16]:

$$\begin{aligned} (N_i, M_i, P_i) &= \int_{-h/2}^{h/2} \sigma_i(1, z, z^3) dz, \quad (i = x, \theta, x\theta) \\ (Q_i, R_i) &= \int_{-h/2}^{h/2} \tau_{iz}(1, z^2) dz, \quad (i = x, \theta) \end{aligned} \quad (16)$$

By placing Eqs. (13) and (11) in Eq. (15), the structural equations for the cylindrical shell will be obtained as follows [40, 44]:

$$\begin{aligned} N_x &= \varepsilon_{xm}A_{11} + k_x B_{11} + k_1 F_{11} + \varepsilon_{\theta m}A_{12} + k_\theta B_{12} \\ &\quad + k_2 F_{12} - A_{11}\alpha_{11}\Delta T - A_{12}\alpha_{22}\Delta T \\ N_\theta &= \varepsilon_{xm}A_{21} + k_x B_{21} + k_1 F_{21} + \varepsilon_{\theta m}A_{22} + k_\theta B_{22} \\ &\quad + k_2 F_{22} - A_{21}\alpha_{11}\Delta T - A_{22}\alpha_{22}\Delta T \\ N_{x\theta} &= \gamma_{x\theta m}A_{66} + 2k_{x\theta}B_{66} + 2k_3F_{66} \end{aligned}$$

$$\begin{aligned}
M_x &= \varepsilon_{xm}B_{11} + k_x D_{11} + k_1 H_{11} + \varepsilon_{\theta m}B_{12} + k_{\theta} D_{12} \\
&\quad + k_2 H_{12} - B_{11}\alpha_{11}\Delta T - B_{12}\alpha_{22}\Delta T \\
M_{\theta} &= \varepsilon_{xm}B_{21} + k_x D_{21} + k_1 H_{21} + \varepsilon_{\theta m}B_{22} + k_{\theta} D_{22} \\
&\quad + k_2 H_{22} - B_{21}\alpha_{11}\Delta T - B_{22}\alpha_{22}\Delta T \\
M_{x\theta} &= \gamma_{x\theta m}B_{66} + 2k_{x\theta}D_{66} + 2k_3H_{66} \\
P_x &= \varepsilon_{xm}F_{11} + k_x H_{11} + k_1 I_{11} + \varepsilon_{\theta m}F_{12} + k_{\theta} H_{12} \\
&\quad + k_2 I_{12} - F_{11}\alpha_{11}\Delta T - F_{12}\alpha_{22}\Delta T \quad (17) \\
P_{\theta} &= \varepsilon_{xm}F_{21} + k_x H_{21} + k_1 I_{21} + \varepsilon_{\theta m}F_{22} + k_{\theta} H_{22} \\
&\quad + k_2 I_{22} - F_{21}\alpha_{11}\Delta T - F_{22}\alpha_{22}\Delta T \\
P_{x\theta} &= \gamma_{x\theta m}F_{66} + 2k_{x\theta}H_{66} + 2k_3I_{66} \\
Q_x &= K\gamma_{xzm}A_{55} + 2Kk_{xz}D_{55} \\
Q_{\theta} &= K\gamma_{\theta zm}A_{44} + 2Kk_{\theta z}D_{44} \\
R_x &= K\gamma_{xzm}D_{55} + 2Kk_{xz}H_{55} \\
R_{\theta} &= K\gamma_{\theta zm}D_{44} + 2Kk_{\theta z}H_{44}
\end{aligned}$$

where in the above relation, the strain coefficients are defined as follows:

$$\begin{aligned}
&(A_{ij}, B_{ij}, D_{ij}, F_{ij}, H_{ij}, I_{ij}) \\
&= \int_{-h_2}^{h_2} Q_{ij}(1, z, z^2, z^3, z^4, z^6) dz \\
&= \int_{-h_2}^{h_2} Q_{ij}(1, z, z^2, z^3, z^4, z^6) dz \quad (18) \\
&\left(\begin{array}{l} i = 1, 2 \\ j = 1, 2 \end{array} \right), \quad (i = j = 4), \quad (i = j = 5), \\
&(i = j = 6)
\end{aligned}$$

Inhomogeneous Q_{ij} is a function of z .

In the above equations, because $Q_{12} = Q_{21}$ and the distribution of nanotubes in the matrix are symmetric to the midplane surface (do not depends on z), therefore:

$$\begin{aligned}
&(B_{ij}, F_{ij}) = 0 \\
&\left(\begin{array}{l} i = 1, 2 \\ j = 1, 2 \end{array} \right), \quad (i = j = 4), \quad (i = j = 5), \quad (19) \\
&(i = j = 6)
\end{aligned}$$

Therefore, according to the above relations, the equations of forces and torques are as follows:

$$\begin{aligned}
&(A_{ij}, D_{ij}, H_{ij}, I_{ij}) = \int_{-h_2}^{h_2} Q_{ij}(1, z^2, z^4, z^6) dz \\
&= \int_{-h_2}^{h_2} Q_{ij}(1, z^2, z^4, z^6) dz \quad (20) \\
&\left(\begin{array}{l} i = 1, 2 \\ j = 1, 2 \end{array} \right), \quad (i = j = 4), \quad (i = j = 5), \\
&(i = j = 6)
\end{aligned}$$

In the present study, the energy method has been used to achieve equilibrium equations. The total potential energy V for the shell, when U is the strain

energy and Ω is the potential energy of the applied mechanical forces (work of external forces) and U_f is the energy caused by the elastic foundation on the shell, then [40]:

$$V = U - \Omega - U_f - U_T \quad (21)$$

The potential energy Ω , when the shell is under the axial load of the compressive edges, is:

$$\Omega = \int \int \frac{P}{\alpha} u_{,x} d\theta dx,$$

The energy from U_f is:

$$U_f = \frac{1}{2} \int_0^L \int_0^\alpha \left[K_w w_0^2 + \frac{1}{a^2} k_g (W_{0,\theta}^2) + K_g w_{0,x}^2 \right] ad\theta dx$$

The energy caused by thermal strain:

$$U_T = \frac{1}{2} \int_0^L \int_0^\alpha \int_{-h/2}^{h/2} (\sigma_{xx}\alpha_{11} + \sigma_{\theta\theta}\alpha_{22}) \Delta T \, adzd\theta dx$$

Therefore, the total potential energy can be written as follows:

$$\begin{aligned}
V &= \frac{1}{2} \int_0^L \int_0^\alpha \int_{-\frac{h}{2}}^{\frac{h}{2}} [\sigma_x \varepsilon_x + \sigma_\theta \varepsilon_\theta + \sigma_{x\theta} \varepsilon_{x\theta} \\
&\quad + \sigma_{xz} \varepsilon_{xz} + \sigma_{\theta z} \varepsilon_{\theta z} - (\sigma_{xx}\alpha_{11} + \sigma_{\theta\theta}\alpha_{22}) \Delta T] dz d\theta dx \\
&\quad - \frac{1}{2} \int_0^L \int_0^\alpha \left[K_w w_0^2 + \frac{1}{a^2} k_g (W_{0,\theta}^2) + K_g w_{0,x}^2 \right] ad\theta dx \\
&\quad + \int_0^L \int_0^\alpha \frac{P}{\alpha} u_{,x} d\theta dx, \quad (22)
\end{aligned}$$

On the other hand, the functional of the total potential energy is as follows:

$$V = \int \int F dx d\theta$$

By substituting Eqs. (14) and (11) in Eq. (20) and applying the minimum energy principle to the function of the total potential energy by using the Euler equations, equilibrium equations are obtained as follows (For the sake of brevity, details on deriving the equilibrium equations are given in appendix A.):

$$\begin{aligned}
&aN_{x,x} + N_{x\theta,\theta} = 0 \\
&aN_{\theta,x} + N_{\theta,\theta} = 0 \\
&-N_\theta + aw_{,xx}N_x + 2w_{,x\theta}N_{x\theta} + aQ_{x,x} - \frac{4a}{h^2}R_{x,x} \\
&\quad + \frac{1}{a}w_{,\theta\theta}N_\theta + Q_{\theta,\theta} - \frac{4}{h^2}R_{\theta,\theta} + \frac{4}{3h^2}aP_{x,xx} \\
&\quad + \frac{4}{3ah^2}P_{\theta,\theta\theta} + \frac{8}{3h^2}P_{x\theta,x\theta} \\
&\quad + ak_g \left(w_{0,xx} + \frac{1}{a^2}w_{0,\theta\theta} \right) - ak_w w_0 = -aP_e
\end{aligned}$$

$$\begin{aligned}
 & -aQ_x + \frac{4}{h^2}aR_x + aM_{x,x} - \frac{4}{3h^2}aP_{x,x} + M_{x\theta,\theta} \\
 & - \frac{4}{3h^2}P_{x\theta,\theta} = 0 \\
 & -aQ_\theta + \frac{4}{h^2}aR_\theta + aM_{x\theta,x} - \frac{4}{3h^2}aP_{x\theta,x} + M_{\theta,\theta} \\
 & - \frac{4}{3h^2}P_{\theta,\theta} = 0
 \end{aligned} \tag{23}$$

The stability equations of single-walled carbon nanotubes reinforced cylindrical panels on elastic foundation subjected to mechanical loads based of TSDT are obtained in this section. Consider V as the total energy of the panel, Taylor expansion of the total energy of the panel V is such that:

$$\Delta V = \delta V + \frac{1}{2!}\delta^2 V + \frac{1}{3!}\delta^3 V$$

In fact, δV (first variation of the total energy) is related to equilibrium of the structure and the $\delta^2 V$ is the original form of the stability in adjacent equilibrium position.

$$\delta(\delta^2 V) = 0$$

Equilibrium equations are nonlinear and because of this reason we derive the stability equations. To investigate the possibility of equilibrium in the adjacent position, the components of displacements on the primary equilibrium path are perturbed infinitesimally to establish an adjacent equilibrium position, then the new format of displacement components is substituted into equilibrium equations to obtain the stability critical load of the cylindrical panel which is in stable equilibrium position that is expressed by u_0, v_0, w_0, φ_0 , and Ψ_0 displacements. Therefore, displacement components associated to the secondary equilibrium path are:

$$\begin{aligned}
 u &= u_0 + u_1 & v &= v_0 + v_1 & w &= w_0 + w_1 \\
 u_1 &= \varphi_0 + \varphi_1 & v_1 &= \Psi_0 + \Psi_1
 \end{aligned} \tag{24}$$

Additionally, the values of the stress resultants depend on adjacent equilibrium position as:

$$\begin{aligned}
 N_x &= N_{x0} + \Delta N_x, & P_x &= P_{x0} + \Delta P_x, \\
 N_x &= N_{x0} + \Delta N_x, & P_x &= P_{x0} + \Delta P_x, \\
 R_x &= R_{x0} + \Delta R_x & N_\theta &= N_{\theta0} + \Delta N_\theta, \\
 P_\theta &= P_{\theta0} + \Delta P_\theta, & R_\theta &= R_{\theta0} + \Delta R_\theta \\
 N_{x\theta} &= N_{x\theta0} + \Delta N_{x\theta}, & P_{x\theta} &= P_{x\theta0} + \Delta P_{x\theta} \\
 M_x &= M_{x0} + \Delta M_x, & Q_x &= Q_{x0} + \Delta Q_x \\
 M_\theta &= M_{\theta0} + \Delta M_\theta, & Q_\theta &= Q_{\theta0} + \Delta Q_\theta, \\
 M_{x\theta} &= M_{x\theta0} + \Delta M_{x\theta}
 \end{aligned} \tag{25}$$

$R_{\theta1}, R_{x1}, P_{x\theta1}, P_{\theta1}, M_{x\theta1}, M_{\theta1}, M_{x1}, Q_{\theta1}, Q_{x1}, N_{x\theta1}, N_{\theta1}, N_{x1}$ are the linear part of the $\Delta R_\theta, \Delta R_x, \Delta P_{x\theta}$,

$\Delta P_\theta, \Delta P_x, \Delta M_{x\theta}, \Delta M_\theta, \Delta M_x, \Delta Q_\theta, \Delta Q_x, \Delta N_{x\theta}, \Delta N_\theta, \Delta N_x$ are going to explain.

$R_{\theta1}, R_{x1}, P_{x\theta1}, P_{\theta1}, P_{x1}, M_{x\theta1}, M_{\theta1}, M_{x1}, Q_{\theta1}, Q_{x1}, N_{x\theta1}, N_{\theta1}, N_{x1}$ are functions of $\psi_1, \varphi_1, w_1, v_1, u_1$ displacements.

where the subscript (0) represents the equilibrium position, and the subscript (1) represents an infinitesimally perturbation. For the sake of brevity, complete strain and stress resultant expressions are given in appendix B.

By substituting strain components given in appendix B, in Eq. (22) and by powering second order terms, the second variation of potential energy is obtained as:

$$\begin{aligned}
 \frac{1}{2}\delta^2 V &= \int_0^L \int_0^{2\pi} \{ [(\varepsilon_{xm0} + \varepsilon_{xm1}) N_x + (k_{x0} + k_{x1}) M_x \\
 & + (k_{10} + k_{11}) P_x] \\
 & + [(\varepsilon_{\theta m0} + \varepsilon_{\theta m1}) N_\theta + (k_{\theta0} + k_{\theta1}) M_\theta \\
 & + (k_{20} + k_{21}) P_\theta] + [(\gamma_{x\theta m0} + \gamma_{x\theta m1}) N_{x\theta} \\
 & + 2(k_{x\theta0} + k_{x\theta1}) M_{x\theta} + 2(k_{30} + k_{31}) P_{x\theta}] \\
 & + 1[(\gamma_{Xzm0} + \gamma_{x\theta m1}) Q_x + 2(k_{xz0} + k_{xz1}) R_x] \} \\
 & + 1[(\gamma_{\theta zm0} + \gamma_{\theta m1}) Q_\theta + 2(k_{\theta z0} + k_{\theta z1}) \\
 & + \frac{1}{2} [k_w w_1^2 + k_g (w_{1,x})^2 + \frac{1}{a^2} k_g (w_{1,\theta})^2] \} ad\theta dx
 \end{aligned} \tag{26}$$

Therefore the functional F in terms of strain components is given by

$$\begin{aligned}
 F &= \left\{ A_{11}\varepsilon_{xm1}^2 + A_{22}\varepsilon_{\theta m1}^2 + 2A_{12}\varepsilon_{xm1}\varepsilon_{\theta m1} + A_{44}\varepsilon_{\theta zm1}^2 \right. \\
 & + A_{55}\varepsilon_{xzm1}^2 + A_{66}\varepsilon_{x\theta m1}^2 + D_{11}k_{x1}^2 + D_{22}k_{\theta1}^2 \\
 & + 2D_{12}k_{x1}k_{\theta1} + 4D_{44}k_{\theta z1}\varepsilon_{\theta zm1} + 4D_{55}k_{xz1}\varepsilon_{xzm1} \\
 & + 4D_{66}k_{x\theta1}^2 + 2H_{11}k_1k_{x1} + 2H_{22}k_{21}k_{\theta1} \\
 & + 2H_{12}(k_1k_{\theta1} + k_{21}k_{x1}) + 4H_{44}k_{\theta z1}^2 + 4H_{55}k_{xz1}^2 \\
 & + 8H_{66}k_{31}k_{x\theta1} + I_{11}k_1^2 + I_{22}k_{21}^2 + 2I_{12}k_1k_{21} \\
 & + 4I_{66}k_{31}^2 + (A_{11}\varepsilon_{xm0} + A_{12}\varepsilon_{\theta m0})\psi_{x1}^2 \\
 & + (A_{11}\varepsilon_{\theta m0} + A_{12}\varepsilon_{xm0})\psi_{\theta1}^2 \left. + A_{66}\varepsilon_{xm0}\psi_{x1}\psi_{\theta1} \right. \\
 & \left. + \frac{1}{2} \left(k_w w_1^2 + k_g (w_{1,x})^2 + \frac{1}{a^2} k_g (w_{1,\theta})^2 \right) \right\} \tag{27}
 \end{aligned}$$

By use of the functional in Eq. (27) and the Euler equations, the stability equations are obtained as follows:

$$\begin{aligned}
 aN_{x1,x} + N_{x\theta1,\theta} &= 0 \\
 aN_{x\theta1,x} + N_{\theta1,\theta} &= 0
 \end{aligned}$$

$$\begin{aligned}
& -N_{\theta 1} + aw_{1,xx}N_{x0} + 2w_{1,x\theta}N_{x\theta 0} + aQ_{x1,x} - \frac{4}{h^2}aR_{x1,x} \\
& + \frac{1}{a}w_{1,\theta\theta}N_{\theta 0} + 1Q_{\theta 1,\theta} - \frac{4}{h^2}R_{\theta 1,\theta} + \frac{4}{3h^2}aP_{x1,x,x} \\
& + \frac{4}{3ah^2}P_{\theta 1,\theta\theta} + \frac{8}{3h^2}P_{x\theta 1,x\theta} + ak_g \left[w_{1,xx} + \frac{1}{a^2}w_{1,\theta\theta} \right] \\
& - ak_w w_1 = 0 \tag{28}
\end{aligned}$$

$$\begin{aligned}
& -aQ_{x1} + \frac{4}{h^2}aR_{x1} + aM_{x1,x} - \frac{4}{3h^2}aP_{x1,x} + M_{x\theta 1,\theta} \\
& - \frac{4}{3h^2}P_{x\theta 1,\theta} = 0 \\
& -aQ_{\theta 1} + \frac{4}{h^2}aR_{\theta 1} + aM_{x\theta 1,x} - \frac{4}{3h^2}aP_{x\theta 1,x} + M_{\theta 1,\theta} \\
& - \frac{4}{3h^2}P_{\theta 1,\theta} = 0
\end{aligned}$$

where $N_{x\theta 0}$, $N_{\theta 0}$, and N_{x0} are pre-buckling forces.

4. Analysis of the Cylindrical Panel Buckling

Assuming that the shell in question is subjected to a P axial load, the resulting pre-buckling forces are calculated using the following equations [40]:

$$\begin{aligned}
N_{x\theta 0} &= 0, \\
N_{x0} &= 0, \tag{29}
\end{aligned}$$

If the buckling force is mechanical:

$$\begin{aligned}
N_{x\theta 0} &= 0, \\
N_{\theta 0} &= 0, \\
N_{x0} &= -\frac{P}{a\alpha}
\end{aligned}$$

If the pre-buckling force is thermal:

$$N_{x0} = \beta\Delta T = \Delta T \int_{-h/2}^{h/2} (\alpha_{11}Q_{11} + \alpha_{22}Q_{12})dz$$

According to the boundary conditions of the simple support at both ends of the shell, the following equations are established:

$$w_1 = v_1 = N_x = M_x = 0 \tag{30}$$

According to the boundary conditions considered for the shell, the displacement components are equal to the following relations:

$$\begin{aligned}
u_1 &= \sum_{n=1}^{\infty} \sum_{m=1}^{\infty} U_{x0} \sin(\beta_m\theta) \cos(P_n x), \\
v_1 &= \sum_{n=1}^{\infty} \sum_{m=1}^{\infty} U_{\theta 0} \cos(\beta_m\theta) \sin(P_n x), \\
w_1 &= \sum_{n=1}^{\infty} \sum_{m=1}^{\infty} U_{z0} \sin(\beta_m\theta) \sin(P_n x), \tag{31}
\end{aligned}$$

$$\varphi_1 = \sum_{n=1}^{\infty} \sum_{m=1}^{\infty} U_{x1} \sin(\beta_m\theta) \cos(P_n x),$$

$$\psi_1 = \sum_{n=1}^{\infty} \sum_{m=1}^{\infty} U_{\theta 1} \cos(\beta_m\theta) \sin(P_n x),$$

where:

$$\beta_m = \frac{m\pi}{\alpha}, \quad P_n = \frac{n\pi}{L},$$

which are fixed values. m and n are the numbers of waves in the direction θ and x , and they are $m, n = 1, 2, 3, \dots$. By placing the above solutions in the equations of stability, equations are obtained that can be represented as the following matrix.

$$\begin{bmatrix} a_{11} & a_{12} & a_{13} & a_{14} & a_{15} \\ a_{21} & a_{22} & a_{23} & a_{24} & a_{25} \\ a_{31} & a_{32} & a_{33} & a_{34} & a_{35} \\ a_{41} & a_{42} & a_{43} & a_{44} & a_{45} \\ a_{51} & a_{52} & a_{53} & a_{54} & a_{55} \end{bmatrix} \begin{bmatrix} U_{x0} \\ U_{\theta 0} \\ U_{z0} \\ U_{x1} \\ U_{\theta 1} \end{bmatrix} = \begin{bmatrix} 0 \\ 0 \\ 0 \\ 0 \\ 0 \end{bmatrix} \tag{32}$$

The condition for having a non-zero solution for the system of Eq. (32) is that the determinant of the coefficients is equal to zero. By obtaining the load and buckling temperature in terms of functions of parameters m and n and minimizing it to these two parameters, the critical buckling temperature load will be obtained.

5. Numerical Results

This section presents thermo-mechanical buckling of nanocomposite shell with polymethyl methacrylate matrix reinforced with single-walled carbon nanotubes (10,10) under simple support conditions under compressive and thermal axial loading effect, in two states of uniform distribution, and non-uniform (graded) distribution of nanotubes are discussed. For this purpose, it is first needed to characterize the material attributes of carbon-reinforced composite nanotubes. Moreover, to make the reinforced structure more specific, the distribution of nanotubes in the shell section is shown in Fig. 3. The properties of carbon nanotubes of type (10,10) are listed in Table 4, where L is the length, R is the radius, h is the thickness, and ν is the Poisson's ratio. Table 3 also shows the dependence of the elastic and shear modulus of carbon nanotubes on temperature. In this paper, the values are considered at room temperature (300k).

In Tables 1, 2, and 3, a comparative study has been done between the present work and the references [40, 49–51] to prove the correctness of the research.

Table 1

Buckling critical temperature (k) for isotropic cylindrical shell exposed to the uniform heat load.

Homogenous	E (GPa)	μ	[37]	Present work
Alumina	380	0.3	19.672	19.6721
Aluminum	70	0.3	3.6238	3.6253

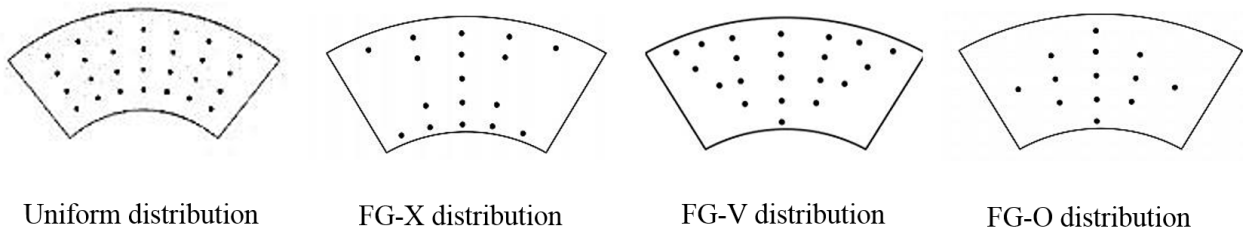


Fig. 3. The distribution of nanotubes in the section of the panel.

Table 2

Buckling critical temperature (k) for isotropic cylindrical shell exposed to the uniform heat load.

Homo- genous	E (GPa)	μ	α $10^{-6} \frac{1}{K}$	[46]	[47]	Present work
Alumina	380	0.3	7.4	567.8	597.2	559.24
Aluminum	70	0.3	23	182.6	187.3	183.31

Table 3

Critical buckling temperature (K) for cylindrical shell reinforced with carbon nanotubes exposed to the uniform heat load
Subject matter PMMA ($\frac{l}{a} = 1$, $\frac{h}{a} = 0.01$, $a = 0.5m$, $V_{CN} = 0.12$, $\alpha = 2\pi$).

Subject matter	E (GPa)	μ	α $10^{-6} \frac{1}{K}$	V_{CN}	[48]	Present work
				0.12	31.749	32.251
PMMA	2.5	0.34	45	0.17	37.346	41.792
				0.28	32.110	31.505

Table 4

Material properties of single-walled carbon nanotubes (10,10) [15].

Type of tubes	L	R	h	v_{12}^{CN}
SWCNT (10,10)	9.26Nm	0.68Nm	0.067Nm	0.175

Table 5

Dependence of material properties of single-walled carbon nanotubes (10,10) [15]
We also have a polymethacrylate (PMMA) matrix for material properties [15]
 $E^m = 2.5GPa$, $G^m = 0.933GPa$, $\nu^m = 0.34$.

Temp. (k)	E_{11}^{CN} (TPa)	E_{22}^{CN} (TPa)	G_{12}^{CN} (TPa)
300	5.6466	7.0800	1.9445
500	5.5308	6.9348	1.9643
700	5.4744	6.8641	1.9644
1000	5.2814	6.6220	1.9451

As shown in Table 6, the improved rules of mixtures are in worthy compliance with the results of molecular dynamics. However, for more accurate values, the efficiency coefficient of nanotubes can be deliberated by the rules of mixtures and the results of molecular dynamics. Based on previous research in the field of

nanocomposites, in the present study, the hypotheses $G_{12} = G_{23} = G_{13}$ and $\eta_3 = \eta_2$ have been considered.

Fig. 4 illustrates critical load for different distributions of carbon nanotubes versus h/a for $V_{CNT} = 0.28$. As seen in Fig. 4, the FG-X distribution results in the most critical load and and the FG-O distributions result in the lowest amount of critical load. Figs. 5 and 6 show the critical buckling load values for the cylindrical panel reinforced with single-walled carbon nanotubes of type (10,10) under axial load, in uniform (UD) and non-uniform distribution (FG) for different amount of the volume deduction of carbon nanotubes in terms of parameters l/a (length/radius) and h/a (thickness/radius). Furthermore, Fig. 7 shows the buckling load of the shell with its opening angle. Fig. 8 illustrates an evaluation between the buckling load of the shell in the existence of elastic basis for a volume fraction of 0.12 in the FG and UD states of the nanotubes. Fig. 9 compares the effect between homogeneity and heterogeneity of the nanocomposite matrix on the critical buckling temperature.

Table 6

Results of molecular dynamics and rules of mixtures [15].

V_{CN}	Molecular dynamics			Rules of mixtures		
	E_{11} (TPa)	E_{22} (TPa)	E_{11} (TPa)	η_1	E_{22} (TPa)	η_2
0.12	94.6	2.9	78.94	0.137	2.9	1.022
0.17	138.9	4.9	68.138	0.142	4.9	1.626
0.28	224.2	5.5	224.50	0.141	5.5	11.585

Figs. 10 and 11 show that critical load increases by increasing the amount of Pasternak and Winkler coefficients. Fig. 12 depicts critical temperature for different distributions of carbon nanotubes versus h/a for $V_{CNT} = 0.28$. As seen in Fig. 12, the FG-X distribution results in the highest critical temperature and the FG-O distribution results in the lowest amount of critical temperature.

Figs. 13 and 14 show the critical buckling temperature values for the cylindrical panel reinforced with SWCNs of type (10,10) under heat load, in uniform(UD) and non-uniform(FG) states, respectively, for different amount of volume deduction of carbon nanotubes in terms of parameters l/a (length/radius) and h/a (thickness/radius).

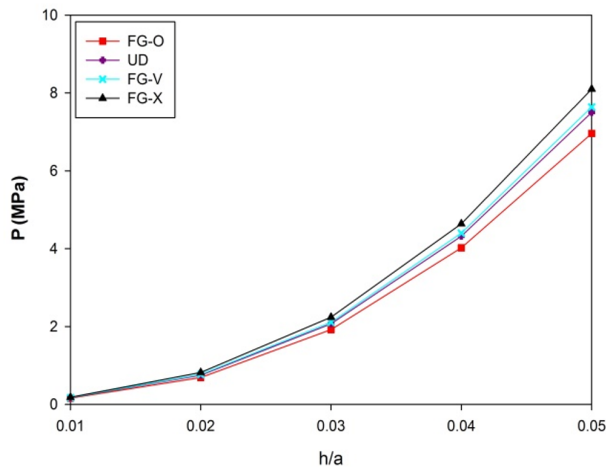


Fig. 4. Results of critical buckling load for different distributions of nanotubes ($V_{CNT} = 0.28$, $l = a = 1\text{m}$, $\alpha = \frac{\pi}{6}$, $k_g = 10$, $k_w = 100$, $\mu' = 0.4$).

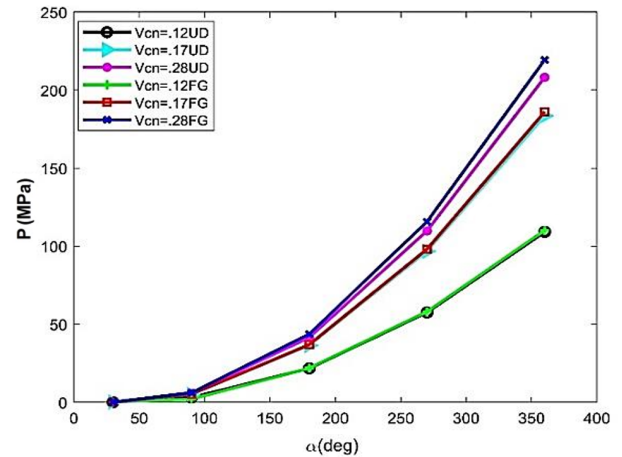


Fig. 7. Critical buckling load in terms of panel span angle in FG and UD distributions of nanotubes ($a = 1\text{m}$, $\frac{l}{a} = 1$, $\frac{h}{a} = 0.01$, $k_g = 10$, $k_w = 100$, $\mu' = 0.4$).

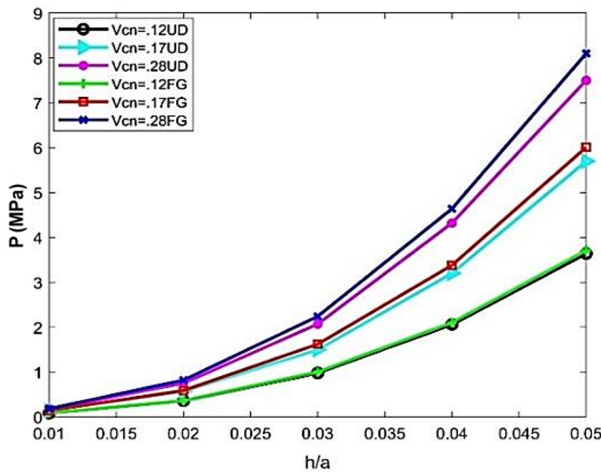


Fig. 5. Results of critical buckling load in l/a in FG and UD distributions of nanotubes ($l = a = 1\text{m}$, $\alpha = \frac{\pi}{6}$, $k_g = 10$, $k_w = 100$, $\mu' = 0.4$).

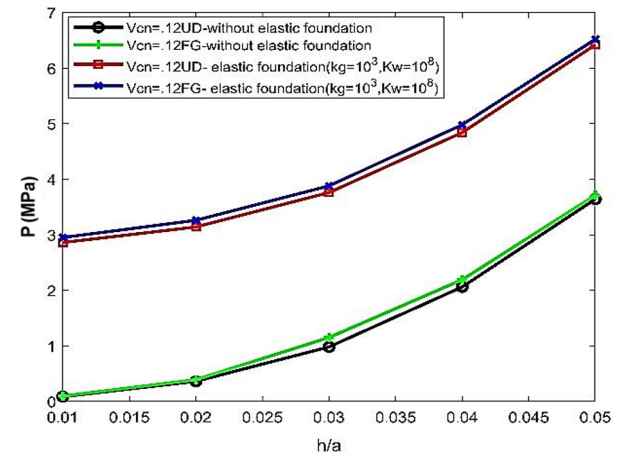


Fig. 8. Results of critical buckling load in h/a for the presence or absence of elastic foundation in the distribution of FG and UD nanotubes.

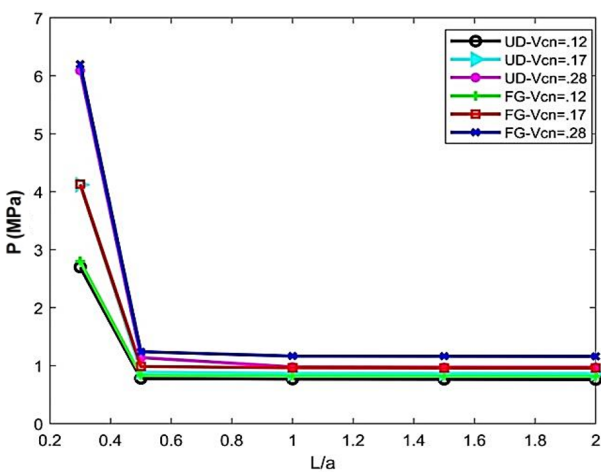


Fig. 6. Results of critical load in l/a in the FG and UD distributions of nanotubes ($a = 1\text{m}$, $\frac{h}{a} = 0.01$, $\alpha = \frac{\pi}{6}$, $k_g = 10$, $k_w = 100$, $\mu' = 0.4$).

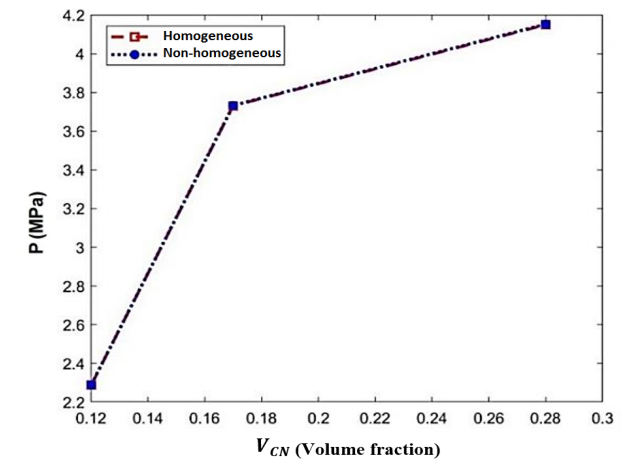


Fig. 9. Comparison between the effect of homogeneity and non-homogeneity of nanocomposite matrix on critical buckling load in terms of volume fraction ($a = 1\text{m}$, $\frac{l}{a} = 1$, $\frac{h}{a} = 0.04$, $k_g = 10$, $k_w = 100$, $\mu' = 0.4$).

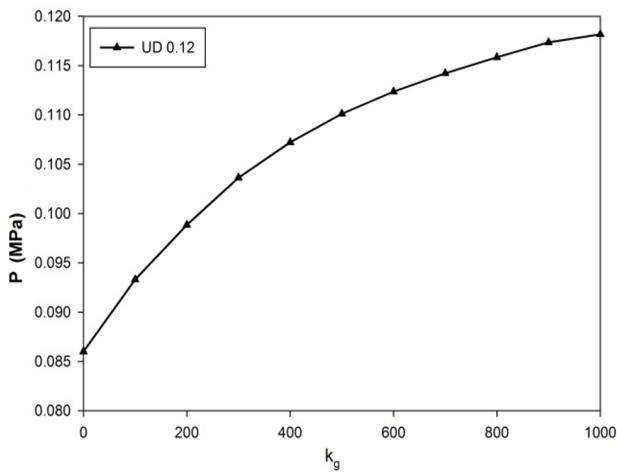


Fig. 10. Critical buckling load in terms of Pasternak coefficient for uniform distribution ($a = 1\text{m}$, $\frac{l}{a} = 1$, $\frac{h}{a} = 0.01$, $k_w = 0$, $\mu' = 0.4$).

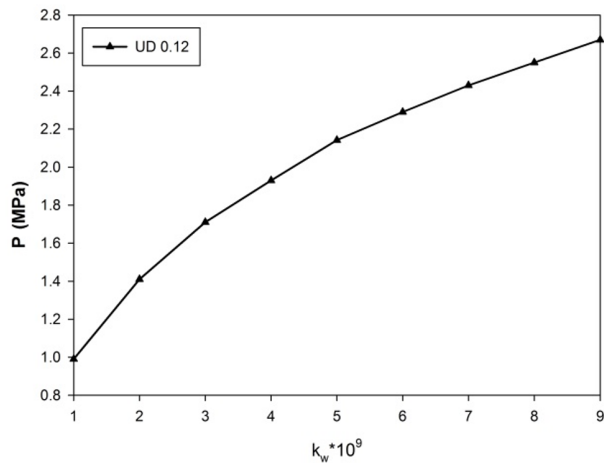


Fig. 11. Critical buckling load in terms of Winkler coefficient for uniform distribution ($a = 1\text{m}$, $\frac{l}{a} = 1$, $\frac{h}{a} = 0.01$, $k_g = 0$, $\mu' = 0.4$).

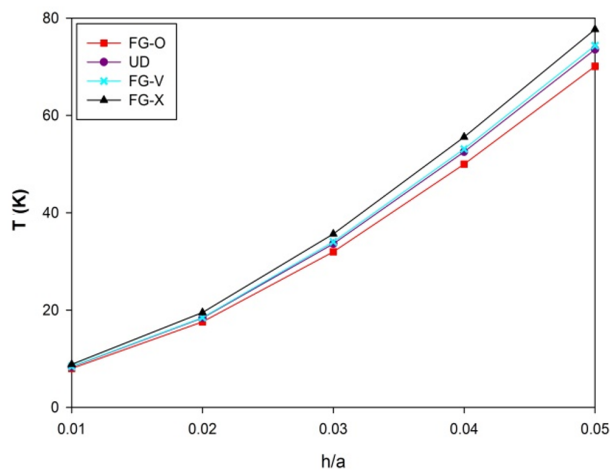


Fig. 12. Results of critical buckling temperature for different distributions of nanotubes ($V_{CNT} = 0.28$, $l = a = 1\text{m}$, $\alpha = \frac{\pi}{6}$, $k_g = 10$, $k_w = 100$, $\mu' = 0.4$).

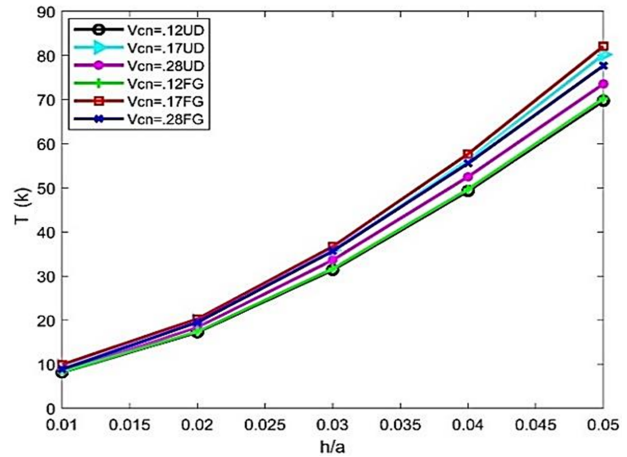


Fig. 13. Results of critical buckling temperature in terms of h/a in the FG and UD distributions of the nanotubes ($l = a = 1\text{m}$, $\alpha = \frac{\pi}{6}$, $k_g = 10$, $k_w = 100$, $\mu' = 0.4$).

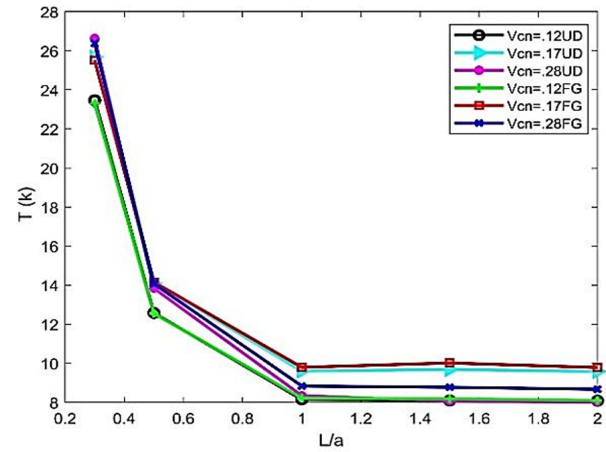


Fig. 14. Results of critical temperature in l/a in the FG and UD distributions of nanotubes ($a = 1\text{m}$, $\frac{h}{a} = 0.01$, $\alpha = \frac{\pi}{6}$, $k_g = 10$, $k_w = 100$, $\mu' = 0.4$).

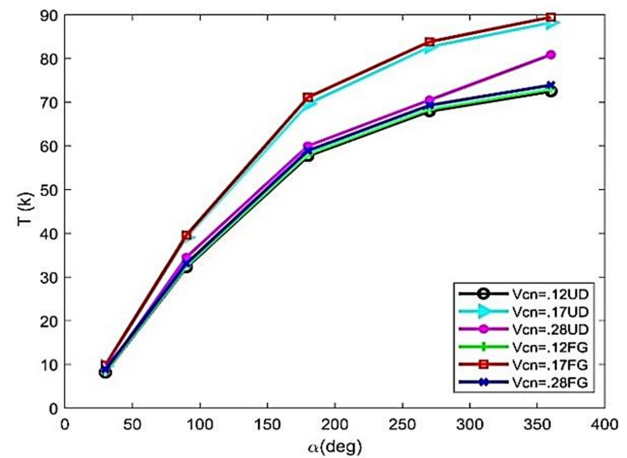


Fig. 15. Results of critical buckling temperature in terms of panel span angle in FG and UD distribution states of nanotubes ($a = 1\text{m}$, $\frac{l}{a} = 1$, $\frac{h}{a} = 0.01$, $k_g = 10$, $k_w = 100$, $\mu' = 0.4$).

Fig. 15 also shows the buckling temperature of the shell in terms of its span angle. Fig. 16 shows a comparison between the critical shell temperature in the existence of a flexible basis for a volume fraction of 0.12 in the FG-X and UD states of the nanotubes. Fig. 17 shows a comparison of the effect between homogeneity and non-homogeneity of nanocomposite matrix on the critical temperature of the buckling.

Figs. 18 and 19 illustrate that the critical temperature increases by growing the amount of Pasternak and Winkler coefficients.

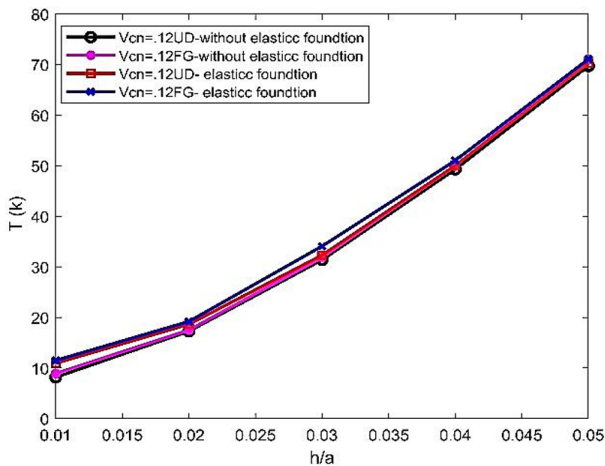


Fig. 16. Results of critical buckling temperature in h/a for the presence or absence of elastic foundation in the FG and UD distribution states of the nanotubes ($k_g = 10^3$, $k_w = 10^6$, $a = 1\text{m}$, $\frac{l}{a} = 1$, $\frac{h}{a} = 0.01$).

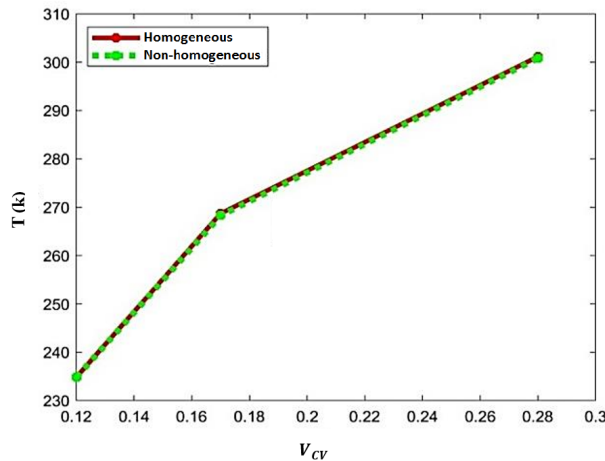


Fig. 17. Comparison between the effect of homogeneity and non-homogeneity of nanocomposite matrix on critical buckling temperature in terms of volume fraction ($a = 1\text{m}$, $\frac{l}{a} = 1$, $\frac{h}{a} = 0.01$, $k_g = 10^3$, $k_w = 10^8$, $\mu' = 0.4$).

6. Conclusions

Thermo-mechanical buckling of composite carbon nanotubes reinforced cylindrical panels under axial pressure and uniform temperature rise was investigated in

the present research. The innovative tips of present work are as follows:

- Use of the third-order theory of shear deformations for modeling.
- Considering a non - homogeneous material.
- Investigation of different nano tubes distributions.
- Effect of elastic substrate on critical mechanical and thermal loads.

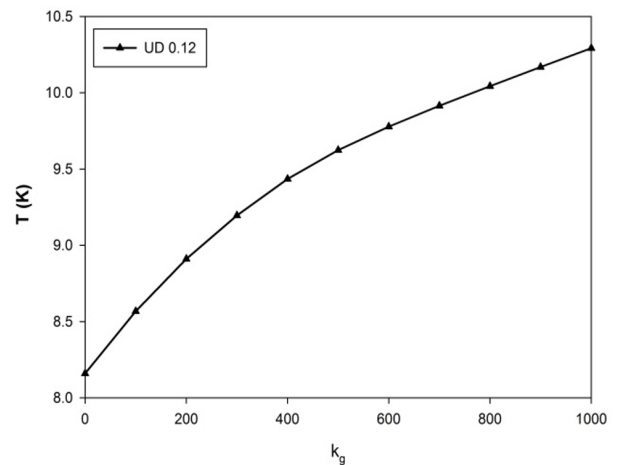


Fig. 18. Critical buckling temperature in terms of Pasternak coefficient for uniform distribution ($a = 1\text{m}$, $\frac{l}{a} = 1$, $\frac{h}{a} = 0.01$, $k_w = 0$, $\mu' = 0.4$).

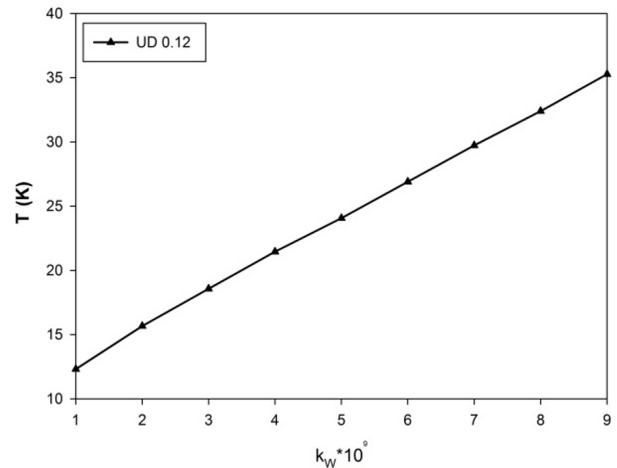


Fig. 19. Critical buckling temperature in terms of Winkler coefficient for uniform distribution ($a = 1\text{m}$, $\frac{l}{a} = 1$, $\frac{h}{a} = 0.01$, $k_g = 0$, $\mu' = 0.4$).

The following issues are concluded from the present analysis:

- By increasing the ratio of thickness to the radius of the shell, in all amounts of the volume deduction of nanotubes, rise in the buckling load is observed. In the state of FG distribution of nanotubes, the buckling load is greater than the state

of uniform distribution. Additionally, by increasing the volume deduction of the nanotube, both in uniform and FG distribution, the critical load increases.

- The FG-X and FG-O distributions result in the highest and lowest amounts of thermal and mechanical critical loads, respectively.
- By increasing the ratio of length to the shell radius at a constant thickness in the state of uniform distribution, the critical load has a sudden decrease to the limit of $L/a < 0.6$, and since then, it remains constant.
- The buckling load increases and reaches its maximum amount in the complete-cylindrical shell by increasing the panel span angle.
- The presence of a flexible basis significantly increases the buckling load.
- Non-homogeneity of the nanocomposite matrix causes a slight increase in the critical buckling load.
- By increasing the ratio of length to the radius of the shell at a constant thickness in the uniform and functionally graded states, the critical temperature decreases abruptly to the limit of $L/a < 0.6$ and remains constant since then.
- By increasing the panel span angle, the buckling temperature increases and reaches its maximum value in a complete cylindrical shell.
- The presence of an elastic foundation causes the critical temperature to increase significantly, where the effect of critical temperature is higher than that of the buckling load.
- Non-homogeneity of the nanocomposite matrix causes a slight reduction of the critical buckling temperature.

Appendix A

$$\begin{aligned}
 V = & \frac{1}{2} \int_0^L \int_0^{2\pi} \int_{-h_2}^{h_2} \left[\sigma_x (\varepsilon_{xm} + zk_x + z^3k_1) \right. \\
 & + \sigma_\theta (\varepsilon_{\theta m} + zk_\theta + z^3k_2) \\
 & + \tau_{x\theta} (\gamma_{x\theta m} + 2zk_{x\theta} + 2z^3k_3) \\
 & + \tau_{xz} (\gamma_{xzm} + 2z^2k_{xz}) \\
 & \left. + \tau_{\theta z} (\gamma_{\theta zm} + 2z^2k_{\theta z}) \right] adz d\theta dx \quad (A.1) \\
 & + \int_0^L \int_0^{2\pi} [(-P_e/a\alpha)w] ad\theta dx \\
 & + \frac{1}{2} \int_0^L \int_0^{2\pi} \left[K_w w_0^2 + K_g \left(w_{0,x}^2 + \frac{1}{a^2} w_{0,\theta}^2 \right) \right] \\
 & ad\theta dx
 \end{aligned}$$

By integrating with respect to z :

$$\begin{aligned}
 V = & \frac{1}{2} \int_0^L \int_0^{2\pi} \left[\left(\varepsilon_{xm} \underbrace{\int_{-\frac{h}{2}}^{\frac{h}{2}} \sigma_x dz}_{N_x} \right. \right. \\
 & \left. \left. + k_x \underbrace{\int_{-\frac{h}{2}}^{\frac{h}{2}} \sigma_x z dz}_{M_x} + k_1 \underbrace{\int_{-\frac{h}{2}}^{\frac{h}{2}} \sigma_x z^3 dz}_{P_x} \right) \right. \\
 & + \left(\varepsilon_{\theta m} \underbrace{\int_{-\frac{h}{2}}^{\frac{h}{2}} \sigma_\theta dz}_{N_\theta} + k_\theta \underbrace{\int_{-\frac{h}{2}}^{\frac{h}{2}} \sigma_\theta z dz}_{M_\theta} \right. \\
 & \left. \left. + k_2 \underbrace{\int_{-\frac{h}{2}}^{\frac{h}{2}} E_{\theta z^3} dz}_{P_\theta} \right) \right. \\
 & + \left(\gamma_{x\theta m} \underbrace{\int_{-\frac{h}{2}}^{\frac{h}{2}} \tau_{x\theta} dz}_{N_{x\theta}} + 2k_{x\theta} \underbrace{\int_{-\frac{h}{2}}^{\frac{h}{2}} \tau_{x\theta} z dz}_{M_{x\theta}} \right. \\
 & \left. \left. + 2k_3 \underbrace{\int_{-\frac{h}{2}}^{\frac{h}{2}} \tau_{x\theta} z^3 dz}_{P_{x\theta}} \right) \right. \\
 & + \left(\gamma_{xzm} \underbrace{\int_{-\frac{h}{2}}^{\frac{h}{2}} \tau_{xz} dz}_{Q_x} + 2k_{xz} \underbrace{\int_{-\frac{h}{2}}^{\frac{h}{2}} \tau_{xz} z^2 dz}_{R_x} \right) \\
 & \left. + \left(\gamma_{\theta zm} \underbrace{\int_{-\frac{h}{2}}^{\frac{h}{2}} \tau_{\theta z} dz}_{Q_\theta} + 2k_{\theta z} \underbrace{\int_{-\frac{h}{2}}^{\frac{h}{2}} \tau_{\theta z} z^2 dz}_{R_\theta} \right) \right] + ad\theta dx \\
 & + \int_0^L \int_0^{2\pi} [-P_e w] ad\theta dx \\
 & + \frac{1}{2} \int_0^L \int_0^{2\pi} \left[K_w w_0^2 + K_g \left(w_{0,x}^2 + \frac{1}{a^2} w_{0,\theta}^2 \right) \right] \\
 & ad\theta dx \quad (A.2)
 \end{aligned}$$

Therefore

$$\begin{aligned}
 V = & \int_0^L \int_0^{2\pi} \frac{1}{2} \left[\left(\varepsilon_{xm} N_x + k_x M_x + k_1 P_x \right) \right. \\
 & + \left(\varepsilon_{\theta m} N_\theta + k_\theta M_\theta + k_2 P_\theta \right) \\
 & + \left(\gamma_{x\theta m} N_{x\theta} + 2k_{x\theta} M_{x\theta} + 2k_3 P_{x\theta} \right) \\
 & + \left(\gamma_{xzm} Q_x + 2k_{xz} R_x \right) \\
 & \left. + \left(\gamma_{\theta zm} Q_\theta + 2k_{\theta z} R_\theta \right) \right] ad\theta dx \quad (A.3)
 \end{aligned}$$

$$\begin{aligned}
& \left. - 2P_e w + K_w w_0^2 + \frac{1}{a^2} k_g (W_{0,\theta}^2) + K_g w_{0,x}^2 \right] \\
& \quad ad\theta dx \\
V = & \int_0^L \int_0^{2\pi} \frac{1}{2} [F] ad\theta dx \\
= & \int_0^L \int_0^{2\pi} \frac{1}{2} F(u_0, v_0, w, u_{0,\theta}, v_{0,x}, v_{0,\theta}, v_x, w_\theta, w_{xx}, \\
& \quad v_{\theta\theta}, w_{x\theta}) ad\theta dx \quad (A.4)
\end{aligned}$$

Therefore the functional F is obtained as follow:

$$\begin{aligned}
F = & \frac{1}{2} (\varepsilon_{xm} N_x + k_x M_x + k_1 P_x) \\
& + \frac{1}{2} (\varepsilon_{\theta m} N_\theta + k_\theta M_\theta + k_2 P_\theta) \\
& + \frac{1}{2} (\gamma_{x\theta m} N_{x\theta} + 2k_{x\theta} M_{x\theta} + 2k_3 P_{x\theta}) \\
& + \frac{1}{2} (\gamma_{xz m} Q_x + 2k_{xz} R_x) \quad (A.5) \\
& + \frac{1}{2} (\gamma_{\theta z m} Q_\theta + 2k_{\theta z} R_\theta) - P_e w \\
& + \frac{1}{2} \left(K_w w_0^2 + \frac{1}{a^2} k_g (W_{0,\theta}^2) + K_g w_{0,x}^2 \right)
\end{aligned}$$

With the aid of Eqs. (12) and (17), the functional F obtained in terms of displacement components as follow:

$$\begin{aligned}
F = & \frac{1}{2} \left(u_{0,x} + \frac{1}{2} w_{,x}^2 \right) \left\{ \left(u_{0,x} + \frac{1}{2} w_{,x}^2 \right) A_{11} \right. \\
& + \left. \left[\frac{v_{0,\theta} + w}{a} + \frac{1}{2} \left(\frac{-w_{,\theta}}{a} \right)^2 \right] A_{12} \right\} \\
& + \frac{1}{2} u_{1,x} \left[u_{1,x} D_{11} - c_\circ (u_{1,x} + w_{,xx}) H_{11} \right. \\
& + \left. \frac{v_{1,\theta}}{a} D_{12} - \frac{c_\circ}{a} \left(v_{1,\theta} + \frac{w_{,\theta\theta}}{a} \right) H_{12} \right] \\
& - \frac{1}{2} c_\circ (u_{1,x} + w_{,xx}) \left[u_{1,x} H_{11} - c_\circ (u_{1,x} + w_{,xx}) I_{11} \right. \\
& + \left. \frac{v_{1,\theta}}{a} H_{12} - \frac{c_\circ}{a} \left(v_{1,\theta} + \frac{w_{,\theta\theta}}{a} \right) I_{12} \right] \\
& + \frac{1}{2} \left[\frac{v_{0,\theta} + w}{a} + \frac{1}{2} \left(\frac{-w_{,\theta}}{a} \right)^2 \right] \\
& \left\{ \left(u_{0,x} + \frac{1}{2} w_{,x}^2 \right) A_{21} \right. \\
& + \left. \left[\frac{v_{0,\theta} + w}{a} + \frac{1}{2} \left(\frac{-w_{,\theta}}{a} \right)^2 \right] A_{22} \right\} \\
& + \frac{v_{1,\theta}}{2a} \left[u_{1,x} D_{21} - c_\circ (u_{1,x} + w_{,xx}) H_{21} \right.
\end{aligned}$$

$$\begin{aligned}
& + \left. \frac{v_{1,\theta}}{a} D_{22} - \frac{c_\circ}{a} \left(v_{1,\theta} + \frac{w_{,\theta\theta}}{a} \right) H_{22} \right] \quad (A.6) \\
& - \frac{c_\circ}{2a} \left(v_{1,\theta} + \frac{w_{,\theta\theta}}{a} \right) \left[u_{1,x} H_{21} - c_\circ (u_{1,x} + w_{,xx}) I_{21} \right. \\
& + \left. \frac{v_{1,\theta}}{a} H_{22} - \frac{c_\circ}{a} \left(v_{1,\theta} + \frac{w_{,\theta\theta}}{a} \right) I_{22} \right] \\
& + \frac{1}{2} \left[\frac{u_{0,\theta}}{a} + v_{0,x} + \left(\frac{+w_{,x} w_{,\theta}}{a} \right) \right]^2 A_{66} \\
& + \frac{1}{2} \left(\frac{u_{1,\theta}}{a} v_{1,x} \right) \left[\left(\frac{u_{1,\theta}}{a} + v_{1,x} \right) D_{66} \right. \\
& - \left. c_\circ \left(\frac{u_{1,\theta}}{a} + v_{1,x} + \frac{2w_{,x\theta}}{a} \right) H_{66} \right] \\
& - \frac{1}{2} c_\circ \left(\frac{u_{1,\theta}}{a} + v_{1,x} + \frac{2w_{,x\theta}}{a} \right) \\
& \left[\left(\frac{u_{1,\theta}}{a} + v_{1,x} \right) H_{66} - c_\circ \left(\frac{u_{1,\theta}}{a} + v_{1,x} + \frac{2w_{,x\theta}}{a} \right) I_{66} \right] \\
& + \frac{1}{2} (u_1 + w_{,x}) [(u_1 + w_{,x}) A_{55} - 3c_\circ (u_1 + w_{,x}) D_{55}] \\
& - \frac{3c_\circ}{2} (u_1 + w_{,x}) [(u_1 + w_{,x}) D_{55} - 3c_\circ (u_1 + w_{,x}) H_{55}] \\
& + \frac{1}{2} \left(v_1 + \frac{w_{,\theta}}{a} \right) \\
& \left[\left(v_1 + \frac{w_{,\theta}}{a} \right) A_{44} - 3c_\circ \left(v_1 + \frac{w_{,\theta}}{a} \right) D_{44} \right] \\
& - \frac{3c_\circ}{2} \left(v_1 + \frac{w_{,\theta}}{a} \right) \\
& \left[\left(v_1 + \frac{w_{,\theta}}{a} \right) D_{44} - 3c_\circ \left(v_1 + \frac{w_{,\theta}}{a} \right) H_{44} \right] \\
& - P_e w + \frac{1}{2} \left[k_w w^2 + k_g \left(w_{0,x}^2 + \frac{1}{a^2} w_{0,\theta}^2 \right) \right]
\end{aligned}$$

Euler Equations are as follow:

$$\begin{aligned}
\frac{\partial F}{\partial u_0} - \frac{\partial}{\partial x} \frac{\partial F}{\partial u_{0,x}} - \frac{\partial}{\partial \theta} \frac{\partial F}{\partial u_{0,\theta}} &= 0 \\
\frac{\partial F}{\partial v_0} - \frac{\partial}{\partial x} \frac{\partial F}{\partial v_{0,x}} - \frac{\partial}{\partial \theta} \frac{\partial F}{\partial v_{0,\theta}} &= 0 \\
\frac{\partial F}{\partial w} - \frac{\partial}{\partial x} \frac{\partial F}{\partial w_{,x}} - \frac{\partial}{\partial \theta} \frac{\partial F}{\partial w_{,\theta}} + \frac{\partial^2}{\partial x^2} \frac{\partial F}{\partial w_{,xx}} \\
&+ \frac{\partial^2}{\partial x \partial \theta} \frac{\partial F}{\partial w_{,x\theta}} + \frac{\partial^2}{\partial \theta^2} \frac{\partial F}{\partial w_{,\theta\theta}} = 0 \quad (A.7) \\
\frac{\partial F}{\partial u_1} - \frac{\partial}{\partial x} \frac{\partial F}{\partial u_{1,x}} - \frac{\partial}{\partial \theta} \frac{\partial F}{\partial u_{1,\theta}} &= 0 \\
\frac{\partial F}{\partial v_1} - \frac{\partial}{\partial x} \frac{\partial F}{\partial v_{1,x}} - \frac{\partial}{\partial \theta} \frac{\partial F}{\partial v_{1,\theta}} &= 0
\end{aligned}$$

Appendix B

The stress resultants at the primary equilibrium position:

$$\begin{aligned}
 N_{x0} &= \varepsilon_{xm0}A_{11} + \varepsilon_{\theta m0}A_{12} \\
 N_{\theta 0} &= \varepsilon_{xm0}A_{21} + \varepsilon_{\theta m0}A_{22} \\
 N_{x\theta 0} &= \gamma_{x\theta m0}A_{66} \\
 M_{x0} &= k_{x0}D_{11} + k_{10}H_{11} + k_{\theta 0}D_{12} + k_{20}H_{12} \\
 M_{\theta 0} &= k_{x0}D_{21} + k_{10}H_{21} + k_{\theta 0}D_{22} + k_{20}H_{22} \\
 M_{x\theta 0} &= 2k_{x\theta 0}D_{66} + 2k_{30}H_{66} \\
 P_{x0} &= k_{x0}H_{11} + k_{10}I_{11} + k_{\theta 0}H_{12} + k_{20}I_{12} \quad (B.1) \\
 P_{\theta 0} &= k_{x0}H_{21} + k_{10}I_{21} + k_{\theta 0}H_{22} + k_{20}I_{22} \\
 P_{x\theta 0} &= 2k_{x\theta 0}H_{66} + 2k_3I_{66} \\
 Q_{x0} &= \gamma_{xzm0}A_{55} + 2k_{xz0}D_{55} \\
 Q_{\theta 0} &= \gamma_{\theta zm0}A_{44} + 2k_{\theta z0}D_{44} \\
 P_{x0} &= \gamma_{xzm0}D_{55} + 2k_{xz0}H_{55} \\
 R_{\theta 0} &= \gamma_{\theta zm0}D_{44} + 2k_{\theta z0}H_{44}
 \end{aligned}$$

Also, the incremental values of the stress resultants are obtained as:

$$\begin{aligned}
 N_{x1} &= \varepsilon_{xm1}A_{11} + \varepsilon_{\theta m1}A_{12} \\
 N_{\theta 1} &= \varepsilon_{xm1}A_{21} + \varepsilon_{\theta m1}A_{22} \\
 N_{x\theta 1} &= \gamma_{x\theta m1}A_{66} \\
 M_{x1} &= k_{x1}D_{11} + k_1H_{11} + k_{\theta 1}D_{12} + k_{21}H_{12} \\
 M_{\theta 1} &= k_{x1}D_{21} + k_1H_{21} + k_{\theta 1}D_{22} + k_{21}H_{22} \\
 M_{x\theta 1} &= 2k_{x\theta 1}D_{66} + 2k_3H_{66} \\
 P_{x1} &= k_{x1}H_{11} + k_1I_{11} + k_{\theta 1}H_{12} + k_{21}I_{12} \quad (B.2) \\
 P_{\theta 1} &= k_{x1}H_{21} + k_1I_{21} + k_{\theta 1}H_{22} + k_{21}I_{22} \\
 P_{x\theta 1} &= 2k_{x\theta 1}H_{66} + 2k_{31}I_{66} \\
 Q_{x1} &= \gamma_{xzm1}A_{55} + 2k_{xz1}D_{55} \\
 Q_{\theta 1} &= \gamma_{\theta zm1}A_{44} + 2k_{\theta z1}D_{44} \\
 R_{x1} &= \gamma_{xzm1}D_{55} + 2k_{xz1}H_{55} \\
 R_{\theta 1} &= \gamma_{\theta zm1}D_{44} + 2k_{\theta z1}H_{44}
 \end{aligned}$$

Linear strain relations for equilibrium state denoted by subscript “0” and the adjacent position by “1”. The strain components are such that:

$$\begin{aligned}
 \varepsilon_{xm} &= \varepsilon_{xm0} + \varepsilon_{xm1}, & k_x &= k_{x0} + k_{x1} \\
 \varepsilon_{\theta m} &= \varepsilon_{\theta m0} + \varepsilon_{\theta m1}, & k_{\theta} &= k_{\theta 0} + k_{\theta 1}, \\
 k_1 &= k_{10} + k_{11} \\
 \gamma_{x\theta m} &= \gamma_{x\theta m0} + \gamma_{x\theta m1}, & k_{x\theta} &= k_{x\theta 0} + k_{x\theta 1}, \\
 k_2 &= k_{20} + k_{21} \quad (B.3)
 \end{aligned}$$

$$\begin{aligned}
 \gamma_{xzm} &= \gamma_{xzm0} + \gamma_{xzm1}, & k_{xz} &= k_{xz0} + k_{xz1}, \\
 k_3 &= k_{30} + k_{31} \\
 \gamma_{\theta zm} &= \gamma_{\theta zm0} + \gamma_{\theta zm1}, & k_{\theta z} &= k_{\theta z0} + k_{\theta z1} \\
 \psi_x &= \psi_{x0} + \psi_{x1}, & \psi_{\theta} &= \psi_{\theta 0} + \psi_{\theta 1}
 \end{aligned}$$

Linear displacements and curvatures in adjacent position are as follow:

$$\begin{aligned}
 \varepsilon_{xm1} &= u_{1,x}, & k_{x1} &= \varphi_{1,x} \\
 \varepsilon_{\theta m1} &= \frac{v_{1,\theta} + w_1}{a}, & k_{\theta 1} &= \frac{\Psi_{1,\theta}}{a} \\
 \gamma_{x\theta m1} &= \frac{u_{1,\theta}}{a} + v_{1,x}, & k_{x\theta 1} &= \frac{1}{2} \left(\frac{\varphi_{1,\theta}}{a} + \Psi_{1,x} \right) \\
 \gamma_{xzm1} &= \varphi_1 + w_{1,x}, & k_{xz1} &= -\frac{3c_0}{2} (\varphi_1 + w_{1,x}) \\
 \gamma_{\theta zm1} &= \Psi_1 + \frac{w_{1,\theta}}{a}, & k_{\theta z1} &= -\frac{3c_0}{2} \left(\Psi_1 + \frac{w_{1,\theta}}{a} \right) \\
 \psi_{x1} &= -w_{1,x}, & k_{11} &= -c_0 (\varphi_{1,x} + w_{1,x,x}) \\
 \psi_{\theta 1} &= \frac{-w_{1,\theta}}{a}, & k_{21} &= -\frac{c_0}{a} \left(\Psi_{1,\theta} + \frac{w_{1,\theta\theta}}{a} \right) \\
 k_{31} &= -\frac{c_0}{2} \left(\frac{\varphi_{1,\theta}}{a} + \Psi_{1,x} + \frac{2w_{1,x\theta}}{a} \right) \quad (B.4)
 \end{aligned}$$

The Euler Equations are as follow:

$$\begin{aligned}
 \frac{\partial F}{\partial u_1} - \frac{\partial}{\partial x} \frac{\partial F}{\partial u_{1,x}} - \frac{\partial}{\partial \theta} \frac{\partial F}{\partial u_{1,\theta}} &= 0 \\
 \frac{\partial F}{\partial v_1} - \frac{\partial}{\partial x} \frac{\partial F}{\partial v_{1,x}} - \frac{\partial}{\partial \theta} \frac{\partial F}{\partial v_{1,\theta}} &= 0 \\
 \frac{\partial F}{\partial w_1} - \frac{\partial}{\partial x} \frac{\partial F}{\partial w_{1,x}} - \frac{\partial}{\partial \theta} \frac{\partial F}{\partial w_{1,\theta}} + \frac{\partial^2}{\partial x^2} \frac{\partial F}{\partial w_{1,xx}} \\
 + \frac{\partial^2}{\partial x \partial \theta} \frac{\partial F}{\partial w_{1,x\theta}} + \frac{\partial^2}{\partial \theta^2} \frac{\partial F}{\partial w_{1,\theta\theta}} &= 0 \quad (B.5) \\
 \frac{\partial F}{\partial \varphi_1} - \frac{\partial}{\partial x} \frac{\partial F}{\partial \varphi_{1,x}} - \frac{\partial}{\partial \theta} \frac{\partial F}{\partial \varphi_{1,\theta}} &= 0 \\
 \frac{\partial F}{\partial \Psi_1} - \frac{\partial}{\partial x} \frac{\partial F}{\partial \Psi_{1,x}} - \frac{\partial}{\partial \theta} \frac{\partial F}{\partial \Psi_{1,\theta}} &= 0
 \end{aligned}$$

References

- [1] C.H. Sun, F. Li, H.M. Cheng, G.Q. Lu, Axial Young's modulus prediction of single walled carbon nanotube arrays with diameters from nanometer to meter scales, *Appl. Phys. Lett.*, 87(19) (2005) 193201.
- [2] J.D. Fidelus, E. Wiesel, F.H. Gojny, K. Schulte, H.D. Wagner, Thermo mechanical properties of randomly oriented carbon/epoxy nanocomposites, *Composites, Part A*, 36(11) (2005) 1555-1561.

- [3] Y.S. Song, J.R. Youn, Modeling of effective elastic properties for polymer based carbon nanotube composites, *Polymer*, 47(5) (2006) 1741-1748.
- [4] Y. Han, J. Elliott, Molecular dynamics simulations of the elastic properties of polymer/carbon nanotube composites, *Comput. Mater. Sci.*, 39(2) (2007) 315-323.
- [5] R. Zhu, E. Pan, A.K. Roy, Molecular dynamics study of the stress-strain behavior of carbon nanotube reinforced Epon862 composites, *Mater. Sci. Eng. A*, 447(1-2) (2007) 51-57.
- [6] M. Gribel, J.M. Hamaekers, Molecular dynamic simulation of the elastic moduli of polymer-carbon nanotube composites, *Comput. Methods Appl. Mech. Eng.*, 193(17-20) (2004) 1773-1788.
- [7] N. Kordani, A. Fereidoon, S. Sadoddin, M. Ghorbanzadeh Ahangari, Investigation of mechanical and thermal behavior of reinforced polypropylene with single walled Carbon nanotube, *Aerospace Mech. J.*, 6(4) (2011) 1-10. (In Persian).
- [8] T. Vodenitcharova, L.C. Zhang, Bending and local buckling of a nanocomposite beam reinforced by a single-walled Carbon nanotube, *Int. J. Solids Struct.*, 43(10) (2006) 3006-3024.
- [9] G. Formica, W. Lacarbonara, R. Alessi, Vibrations of carbon nanotube-reinforced composites, *Sound Vib. J.*, 329(10) (2010) 1875-1889.
- [10] G.D. Seidel, D.C. Lagoudas, Micromechanical analysis of the effective elastic properties of carbon nanotube reinforced composites, *Mech. Mater.*, 38(8-10) (2006) 884-907.
- [11] D. Qian, E.C. Dickey, R. Andrews, T. Rantell, Load transfer and deformation mechanisms in carbon nanotube-polystyrene composites, *Appl. Phys. Lett.*, 76(20) (2000) 2868-2870.
- [12] H.S. Shen, Nonlinear bending of functionally graded Carbon nanotube-reinforced composite plates in thermal environments, *Compos. Struct.*, 91(1) (2009) 9-19.
- [13] H.S. Shen, Z.H. Zhu, Buckling and postbuckling behavior of functionally graded nanotube-reinforced composite plates in thermal environments, *Comput. Mater. Continua*, 18(2) (2010) 155-182.
- [14] L.L. Ke, J. Yang, S. Kitipornchai, Nonlinear free vibration of functionally graded carbon nanotube-reinforced composite beams, *Compos. Struct.*, 92(3) (2010) 676-683.
- [15] M. Raoufi, S. Jafari Mehrabadi, S. Satouri, Free vibration analysis of 2D-FGM annular sectorial moderately thick plate resting on elastic foundation using 2D-DQM solution, *Modares Mech. Eng.*, 14(15) (2015) 299-306.
- [16] M. Mohammadimehr, M. Salami, H. Nasiri, H. Afshari, Thermal effect on deflection, critical buckling load and vibration of nonlocal Euler-Bernoulli beam on Pasternak foundation using Ritz Method, *Modares Mech. Eng.*, 13(11) (2013) 64-76.
- [17] A. Pourasghar, R. Moradi-Dastjerdi, M.H. Yas, A. Ghorbanpour Arani, S. Kamarian, Three-dimensional analysis of carbon nanotube-reinforced cylindrical shells with temperature-dependent properties under thermal environment, *Polym. Compos.*, 39(4) (2018) 1161-1171.
- [18] A. Ghorbanpour Arani, S. Shams, S. Amir, M.J. Maboudi, Buckling of piezoelectric composite cylindrical shell under electro-thermo-mechanical loading, *J. Solid Mech.*, 4(3) (2012) 296-306.
- [19] A.A. Mosallaie Barzoki, A. Ghorbanpour Arani, R. Kolahchi, M.R. Mozdianfard, A. Loghman, Non-linear buckling response of embedded piezoelectric cylindrical shell reinforced with BNNT under electro-thermomechanical loadings using HDQM, *Compos. Part B*, 44(1) (2013) 722-727.
- [20] H.S. Shen, Postbuckling of nanotube-reinforced composite cylindrical shells in thermal environments, Part I: Axially-loaded shells, *Compos. Struct.*, 93(8) (2011) 2096-2108.
- [21] M. Mohammadi, M. Arefi, R. Dimitri, F. Tornabene, Higher-order thermo-elastic analysis of FG-CNTRC cylindrical vessels surrounded by a pasternak foundation, *Nanomaterials*, 9(1) (2019) 79.
- [22] M. Arefi, M. Mohammadi, A. Tabatabaeian, R. Dimitri, F. Tornabene, Two-dimensional thermoelastic analysis of FG-CNTRC cylindrical pressure vessels, *Steel Compos. Struct.*, 27(4) (2018) 525-536.
- [23] M. Arefi, M. Pourjamshidian, A. Ghorbanpour Arani, Application of non-local strain gradient theory and various shear deformation theories to non-linear vibration analysis of sandwich nanobeam with FGCNTRCs face-sheets in electro-thermal environment, *Appl. Phys. A*, 123(5) (2017) 323.
- [24] M. Arefi, E. Mohammad-Rezaei Bidgoli, R. Dimitri, M. Baccocchi, F. Tornabene, Non-local bending analysis of curved nano-beams reinforced by graphene nanoplatelets, *Composites, Part B*, 166 (2019) 1-12.

- [25] M. Arefi, E. Mohammad-Rezaei Bidgoli, R. Dimitri, F. Tornabene, J.N. Reddy, Size-dependent free vibrations of FG polymer composite curved nanobeams reinforced with graphene nanoplatelets resting on pasternak foundations, *Appl. Sci.*, 9(8) (2019) 1580.
- [26] M. Arefi, E. Mohammad-Rezaei Bidgoli, R. Dimitri, F. Tornabene, Free vibrations of functionally graded polymer composite nanoplates reinforced with graphene nanoplatelets, *Aerosp. Sci. Technol.*, 81 (2018) 108-117.
- [27] Y. Tadi Beni, F. Mehralian, H. Razavi, Free vibration analysis of size-dependent shear deformable functionally graded cylindrical shell on the basis of modified couple stress theory, *Compos. Struct.*, 120 (2015) 65-78.
- [28] F. Mehralian, Y. Tadi Beni, Size-dependent torsional buckling analysis of functionally graded cylindrical shell, *Composites, Part B*, 94 (2016) 11-25.
- [29] F. Mehralian, Y. Tadi Beni, R. Ansari, Size dependent buckling analysis of functionally graded piezoelectric cylindrical nanoshell, *Compos. Struct.*, 152 (2016) 45-61.
- [30] H. Zeighampour, Y. Tadi Beni, Size dependent analysis of wave propagation in functionally graded composite cylindrical microshell reinforced by carbon nanotube, *Compos. Struct.*, 179 (2017) 124-131.
- [31] P. Mohammadi Dashtaki, Y. Tadi Beni, Effects of Casimir force and thermal stresses on the buckling of electrostatic nanobridges based on couple stress theory, *Arabian J. Sci. Eng.*, 39(7) (2014) 5753-5763.
- [32] J. Song, B. Karami, D. Shahsavari, Ö. Civalek, Wave dispersion characteristics of graphene reinforced nanocomposite curved viscoelastic panels, *Compos. Struct.*, 277 (2021) 114648.
- [33] M. Khorasani, Z. Soleimani-Javid, E. Arshid, S. Amir, Ö. Civalek, Vibration analysis of graphene nanoplatelets' reinforced composite plates integrated by piezo-electromagnetic patches on the piezo-electromagnetic media, *Waves Random Complex Medium*, (2021) 1-31. <https://doi.org/10.1080/17455030.2021.1956017>.
- [34] M. Karimi Zeverdejani, Y. Tadi Beni, Y. Kiani, Multi-scale buckling and post-buckling analysis of functionally graded laminated composite plates reinforced by defective graphene sheets, *Int. J. Struct. Stab. Dyn.*, 20(01) (2020) 2050001.
- [35] M. Karimi Zeverdejani, Y. Tadi Beni, Effect of laminate configuration on the free vibration/buckling of FG Graphene/PMMA composites, *Adv. Nano Res.*, 8(2) (2020) 103-114.
- [36] E. Bagherizadeh, Y. Kiani, M.R. Eslami, Mechanical buckling of functionally graded material cylindrical shells surrounded by Pasternak elastic foundation, *Compos. Struct.*, 93(11) (2011) 3063-3071.
- [37] H. Babaei, M.R. Eslami, Nonlinear analysis of thermal-mechanical coupling bending of FGP infinite length cylindrical panels based on PNS and NSGT, *Appl. Math. Modell.*, 91 (2021) 1061-1080.
- [38] A. Nosier, M. Ruhi, Three dimensional analysis of laminated cylindrical panels with piezoelectric layers, *Int. J. Eng.*, 19(1) (2006) 61-72.
- [39] A.H. Sofiyev, K. Yucel, M. Avcar, Z. Zerir, The dynamic stability of orthotropic cylindrical shells with nonhomogenous material properties under axial compressive load varying as a parabolic function of time, *J. Reinf. Plast. Compos.*, 25(18) (2006) 1877-1886.
- [40] D.O. Brush, B.O. Almorth, *Buckling of Bars, Plates, and Shells*, New York, McGraw-Hill Publisher, (1975).
- [41] A.M. Zenkour, Maupertuis-lagrange mixed variational formula for laminated composite structures with a refined higher-order beam theory, *Int. J. of Non Linear Mech.*, 32(5) (1997) 989-1001.
- [42] M. Arefi, A.M. Zenkour, A simplified shear and normal deformations non-local theory for bending of functionally graded piezomagnetic sandwich nano-beams in magneto-thermo-electric environment, *J. Sandwich Struct. Mater.*, 18(5) (2016) 624-651.
- [43] M. Arefi, A.M. Zenkour, Free vibration analysis of a three-layered microbeam based on strain gradient theory and three-unknown shear and normal deformation theory, *Steel Compos. Struct.*, 26(4) (2018) 421-437.
- [44] J.N. Reddy, *Mechanics of Laminated Composite Plates and Shells, Theory and Analysis*, Second Edition, Boca Raton, CRC Press LLC, (2004).
- [45] S. Abolghasemi, H.R. Eipakchi, M. Shariati, Analytical solution for buckling of rectangular plates subjected to nonuniform in-plane loadig based on first order shear deformation theory, *Modares Mech. Eng.*, 14(13) (2014) 37-46.
- [46] F. Sohani, H.R. Eipakchi, A survey on free vibration and buckling of a beam with moderately large deflection using first order shear deformation theory, *Modares Mech. Eng.*, 13(14) (2014) 1-14.

- [47] H.S. Shen, C.L. Zhang, Thermal buckling and postbuckling behavior of functionally graded carbon nanotube-reinforced composite plates, *Mater. Des.*, 31(7) (2010) 3403-3411.
- [48] A. Bakhsheshy, K. Khorshidi, Free vibration of functionally graded rectangular nanoplates in thermal environment based on the modified couple stress theory, *Modares Mech. Eng.*, 14(15) (2015) 323-330.
- [49] M. Nejati, R. Dimitri, F. Tornabene, M.H. Yas, Thermal buckling of nanocomposite stiffened cylindrical shells reinforced by functionally graded wavy carbon nanotubes with temperature-dependent properties, *J. Appl. Sci.*, 7(12) (2017) 1223.
- [50] B. Mirzavand, M.R. Eslami, Thermal buckling of imperfect functionally graded cylindrical shells based on the Wan-Donnell model, *J. Therm., Stress*, 29(1) (2006) 37-55.
- [51] O. Miraliyari, M. Bohloli, Thermal buckling of short and long cylindrical shells reinforced with single wall carbon nanotubes using first order shear deformation theory, 2st National Conference on Development of Civil Engineering, Architecture, Electricity and Mechanical in Iran, Gorgan, 17 November (2015).